Report
**R-22-03**
December 2022

# Potential evapotranspiration in boreal forests

## An assessment of different calculation methods

**David Gustafsson**

SVENSK KÄRNBRÄNSLEHANTERING AB

SWEDISH NUCLEAR FUEL
AND WASTE MANAGEMENT CO

Box 3091, SE-169 03 Solna
Phone +46 8 459 84 00
skb.se

SVENSK KÄRNBRÄNSLEHANTERING

ISSN 1402-3091
**SKB R-22-03**
ID 1989360
December 2022

# Potential evapotranspiration in boreal forests

## An assessment of different calculation methods

David Gustafsson, SMHI

*Keywords:* Potential evapotranspiration, Hydrological modelling, Boreal landscapes.

# Abstract

The concept of potential evapotranspiration and different methods to calculate it have been reviewed and assessed using data from three sites on a climatological gradient in Sweden: the SKB investigation site in Forsmark and two ICOS monitoring sites in Norunda and Svartberget/Krycklan.

The Penman equation as implemented by SMHI for the Forsmark area (Penman-SMHI) and used in subsequent hydrological modelling at SKB is shown to generate potential evapotranspiration estimates up to 30 % higher than estimates obtained with a state-of the-art implementation of the Penman-Monteith equation adapted to the properties of a boreal forest landscape. These results confirm previous findings of an apparent overestimation of the potential evapotranspiration by the Penman-SMHI data, when used as input to hydrological modelling of the Forsmark and Krycklan basins.

It is also found that the previous calculation procedures implemented by SMHI underestimate the net radiation input to the Penman equation, and that even higher values of potential evapotranspiration are generated by the Penman equation given correct input data. In fact, the Penman-SMHI estimates are on average close to the reference evapotranspiration method currently recommended by FAO for crop evaporation estimation (albeit with a different seasonal variation). In conclusion, the main reason for the apparent overestimation of the potential evapotranspiration at Forsmark and Krycklan is found to be the Penman equation itself, and its inherent representation of the evapotranspiration of a well-watered short-cut grass.

It is recommended to use a dual-source implementation of the Penman-Monteith equation with parameters adapted to boreal forests landscape characteristics with regard to the land-surface control on water availability (stomata resistance), moisture transport in the atmosphere (aerodynamic resistances) and available energy (net radiation and ground heat flux) and its distribution between canopy and ground. It is further shown how the parameters for using the Penman-Monteith equation could be extracted from an openly available global database of land-surface parameters developed for meteorological model applications, including satellite-based estimates of the leaf area index and tree heights.

# Sammanfattning

Begreppet potentiell evapotranspiration (avdunstning) och ett antal metoder för att beräkna den har granskats och utvärderats med hjälp av data från tre platser i Sverige: SKB:s undersökningsområde i Forsmark och de två ICOS-stationerna i Norunda och Svartberget/Krycklan.

Den så kallade Penmans ekvation så som den använts av SMHI för Forsmarksområdet ger upp emot 30 % högre potentiell evapotranspiration än beräkningar med den så kallade Penman-Monteiths ekvation ifall den senare används med indata anpassade för de nordliga skogslandskap som dominerar undersökningsområdena. Detta bekräftar tidigare undersökningar som indikerat att den potentiella evapotranspirationen beräknad av SMHI enligt Penmans ekvation gav alldeles för höga värden för att användas som indata till hydrologisk modellering av Forsmarks- och Krycklanområdena.

Beräkningsprocedurerna som tidigare använts av SMHI visar sig dock inkludera en underskattning av nettostrålningen som är en av de viktigaste indata till Penmans ekvation. Därmed skulle ännu högre värden av den potentiella avdunstningen ha erhållits om korrekt indata hade använts. I själva verket låg den av SMHI beräknade potentiella evapotranspirationen i medeltal nära resultatet av den av FAO rekommenderade metoden för att beräkna avdunstning från jordbruksgrödor. Denna metod bygger också på den så kallade Penman-Monteiths ekvationen, men med indata anpassade för en typgröda istället för en typisk barrskog.

Slutsatsen är att huvudorsaken till den upplevda överskattningen av den potentiella evapotranspirationen vid Forsmark och Krycklan framförallt kan kopplas till de inneboende egenskaperna i Penmans ekvation – som representerar hur en välvattnad gräsmatta skulle avdunsta under rådande väderförhållanden, vilket väsentligt skiljer sig från en barrskog – och inte till hur ekvationen har använts av SMHI i detta fall.

Rekommendationen är istället att använda Penman-Monteiths ekvation med indata anpassade till ett borealt skogslandskap genom val av parametrar för vegetationen och markytans kontroll av vattentillgång (klyvöppningarnas respons på väderförhållandena), fukttransport i atmosfären (det aerodynamiska motståndet inom och ovan bladverket) och tillgänglig energi (nettostrålning och markvärmeflöde), samt med beräkning av den potentiella evapotranspirationen för vegetation och underliggande mark separat. Det visas vidare hur indata utöver väderdata, som behövs för att använda Penman-Monteiths' ekvation, kan extraheras från en global databas med landyte-parametrar utvecklad för meteorologiska modelltillämpningar. Dessa innehåller bland annat satellitbaserade uppskattningar av bladyteindex och trädhöjd.

# Contents

# 1 Introduction

## 1.1 Background

### 1.1.1 Potential evapotranspiration

**Evapotranspiration (ET)** is a term widely used in hydrology to represent the sum of different evaporation processes contributing to the vapour flux from the land surface to the atmosphere; evaporation of interception (also called canopy evaporation), transpiration, soil evaporation, sublimation of snow and ice, and evaporation from open water surfaces (lakes, rivers). The term is sometimes also applied in hydrological modelling the different evaporation processes by a single ET variable rather than trying to estimate the components separately. Even when evaporation components are estimated separately, it is still common to base the estimates on a common 'reference evapotranspiration' referred to as the 'potential evapotranspiration'. The concept of lumping evaporation processes into 'evapotranspiration' – conceptually or practically – has been criticized since the different evaporation processes – in particular transpiration and canopy evaporation (evaporation of water intercepted on the surface of the vegetation) – may vary in their physical characteristics and response to climatic and land surface conditions (e.g. Savenije 2004).

**Potential evapotranspiration (PET)** is defined as the amount of water that would evaporate and transpire from a land surface if sufficient water is available given the current atmospheric conditions. It is a concept developed in the 1940s by Thornthwaite (1948) and Penman (1948, 1956), and is the most dominating concept used in hydrological models for estimating evaporation (or evapotranspiration). The general idea behind the concept of PET is that there exists a potential (maximum) evaporation governed by the current atmospheric conditions and available energy for evaporation, which can be further adjusted to give the actual evapotranspiration by considering the water availability at the different evaporating land surface elements exposed to this PET. The general approach in many hydrological models is to calculate the ET by scaling the PET with response functions reflecting the impact of e.g. soil moisture conditions. For calculations of different evapotranspiration components using the PET concept, it is further needed to distribute the PET between the components. The distribution of PET between transpiration and soil evaporation is relatively straight-forward, if it is assumed that PET can be partitioned between the vegetation layer and the soil below in a similar way as solar radiation (e.g. Hansen 1984). The distribution of PET between transpiration and canopy evaporation might be more difficult, since their response to the physical conditions may not be adequately represented by a common PET-model as discussed in e.g. Savenije (2004). On the other hand, the wide use of the PET-concept demonstrates its' usefulness to obtain adequate estimates of evaporation and water balance for hydrological modelling purposes (e.g. Shuttleworth 1993, Allen et al. 1998, Oudin et al. 2005, McMahon et al. 2013).

The potential evapotranspiration equation developed by Penman (1948, 1956) and further extended by Monteith (1965) in the form known as the Penman-Monteith equation are probably the most well-known equations, and often used as benchmarks for assessment of more simplified methods such as the temperature index method suggested by Thornthwaite (1948). The Penman-type of equations are physically based models based on the land surface energy balance equation. However fundamental, the usefulness of the Penman type of equations for hydrological modelling has often been questioned due to a higher input data demand compared to more empirical methods based on for instance temperature index only. In fact, the study by Oudin et al. (2005) showed that empirical PET-methods based on air temperature index and seasonal variability represented by extra-terrestrial radiation were more robust than the Penman-type of methods when applied in a hydrological model calibrated to observed runoff for over 300 river basins around the world.

### 1.1.2 Potential evapotranspiration in Sweden

The 1981 SMHI report by Bertil Eriksson (Eriksson 1981): '*The "potential" evapotranspiration in Sweden*' provides a national PET analysis over Sweden for the time period 1961–1978 using meteorological observations from 152 stations over Sweden. It is based on the Penman equation (Penman 1956) with adaptions of the calculation of net radiation to typical Swedish forest conditions with and without snow. Eriksson (1981) acknowledges the limitations of the PET concept already in the first paragraph of the report summary, and points out that evaporation is indeed dependent not only on atmospheric conditions but also on vegetation and soil physical characteristics.

Data from Eriksson (1981) have been used to estimate PET in several studies using the hydrological model HBV ("Hydrologiska Byrån Vattenbalansavdelningen" in Swedish, Bergström 1976), which exemplifies some of the problems with the PET concept. Brandt and Grahn (1998) used the HBV model with PET from Eriksson (1981) as input to estimate evaporation and runoff coefficients over Sweden for the reference period 1961–1990, and identified equifinality between precipitation corrections and parameters in the evaporation routines to be a major problem. Similar issues were discussed by Lindström et al. (1994) who found that the use of a simple temperature index-based PET estimate of Thornthwaite type performed almost as good as the Penman PET estimates. They also point out that the introduction of an explicit interception routine did not improve the model performance. However, it allowed for more realistic snowfall correction factors, implying that the snowfall correction factors in the original HBV model were calibrated to partly represent interception losses. Lindström et al. (1994) also studied the applicability of the Penman PET estimates for lake evaporation. PET calculated according to the original Penman (1948, 1956) are known to underestimate potential lake evaporation since the albedo is adapted for grassland. In addition, the large heat storage capacity of lakes strongly impacts the available energy for evaporation, reducing the PET in spring and increasing it in the autumn. Lindström et al. (1994) found that the modification with a lower albedo by Eriksson (1981) reduced the need for correcting the Penman PET mean levels, but that the seasonal dynamics of lake evaporation requires a delay of about 1 month compared to the Penman equation estimates (peak evaporation shifted from June to July). Subsequently, as input to a water balance model used for estimating groundwater recharge in Sweden, Rohde et al. (2006) developed a temperature-based function for potential evapotranspiration which includes sinusoidal shift of the linear temperature dependence as a function of day of the year. In the original report, Rohde et al. (2006) calibrated this function to potential evapotranspiration data estimated with the Penman (1948) equation for measurement sites in Mid- and Northern Sweden. The same equation has been implemented in the hydrological model HYPE and calibrated for different land cover types in Sweden as part of the S-HYPE model used for national surface water monitoring and flood forecasting (Lindström et al. 2010, Strömqvist et al. 2012).

### 1.1.3 Potential evapotranspiration calculated by SMHI for SKB Forsmark

SMHI has been providing potential evapotranspiration estimation to SKB for the Forsmark study area. The data have been used by SKB as input to the MIKE SHE model to simulate the surface hydrology as part of the site investigation program (Bosson et al. 2008). The PET was calculated with the Penman (1948, 1956) equation following the recommendations from Eriksson (1981) using meteorological observations from the SKB weather stations at Forsmark as input. It will be further referred to as Penman-SMHI in this report.

In the calibration of the MIKE SHE model to the Forsmark area, it was observed that the Penman-SMHI data had to be reduced with a factor of about 0.85 in order to get an acceptable model performance while keeping other model parameters affecting the water balance within reasonable ranges (Bosson et al. 2008). In a similar study in the Krycklan catchment in Northern Sweden, Jutebring Sterte et al. (2018) had to reduce potential evapotranspiration based on the Penman (1948, 1956) equation with a factor of 0.5. This seemingly over-prediction of PET by the Penman equation for boreal landscapes is problematic and there is a need to understand whether or not 1) the Penman PET-equation has been used correctly in the production of the PET data for Forsmark, 2) the Penman PET-equation is at all relevant for boreal landscapes such as the Forsmark and Krycklan study areas, and 3) it is possible to suggest an alternative PET estimate or alternative evaporation scheme for the SKB application of MIKE SHE model in Forsmark.

## 1.2 Objectives

The objectives of this study are to:

- Review the concept of PET and its use in hydrological modelling.
- Investigate if the PET data calculated by SMHI for SKB (Penman-SMHI) are unreasonably high as experienced when used in the MIKE SHE modelling for Forsmark and Krycklan – and if so, identify the reason to why this is the case.
- Suggest an alternative process-based PET model for hydrological modelling of boreal and sub-arctic ecosystems/landscapes.

# 2 Material and methods

## 2.1 Potential evapotranspiration methods

Regardless which evaporation component we consider, it is dependent on three key controlling factors: 1) the available energy needed for the phase change of water from liquid or solid to gas, 2) the availability of water, and 3) the efficiency in the water vapour transport away from the evaporating surface. Depending on climate, vegetation type and density, geology and other land surface characteristics, these 3 factors can have different spatial and temporal patterns that may be represented more or less good by various types of model formulations. In an evaporation framework defined by these 3 key factors, it may seem natural to define the 'potential evapotranspiration' as a function of the available energy and the efficiency in the transport only, if unlimited water availability is assumed. However, even with unlimited water available, there can be surface dependent controls on the availability of water for the evaporation process. The leaves of green plants are covered by microscopic openings called stomata, to enable gas exchange with the atmosphere. To avoid excessive loss of water through the stomata or to enhance the inflow of carbon dioxide, the plants are able to open and close the stomata and, as such, provide a good example of a control on water availability for transpiration. Typically, the stomata response can be related to soil water availability, light, humidity, and temperature conditions.

Depending on the level of complexity and physical basis for an evaporation model, the 3 key factors controlling evaporation is represented in different ways, either explicitly as part of the input variables or sub-components of the equations, or implicitly through the model parameters. In so-called temperature-index models, air temperature is used as a proxy for the available energy for evaporation, and the impact of water availability and transport efficiency are for instance as in its most simple linear form lumped into a temperature evaporation coefficient $c$, so that $PET = cT$. As further demonstrated in the following sections, in more advanced functions such as the Penman or Penman-Monteith equations, all 3 factors are represented explicitly by different components of the equations, using more or less physically-based relations and various meteorological and land surface conditions as input variables.

### 2.1.1 Penman

The basis for the Penman (1948, 1956) equation is the land surface energy balance equation which can be formulated as:

$$R_n = H + LE + G \qquad \text{Equation 2-1}$$

where $R_n$ (MJ m$^{-2}$ day$^{-1}$) is net radiation, $H$ (MJ m$^{-2}$ day$^{-1}$) and $LE$ (MJ m$^{-2}$ day$^{-1}$) are the sensible and latent heat fluxes from the evaporating surface to the atmosphere and $G$ (MJ m$^{-2}$ day$^{-1}$) is the conductive heat flux into the ground. The units are energy per surface area and time, for instance W m$^{-2}$ or MJ m$^{-2}$ day$^{-1}$. The latter is most convenient when converting $LE$ (MJ m$^{-2}$ day$^{-1}$) into the (daily) mass of evaporating water $E$ (kg m$^{-2}$ day$^{-1}$ or mm day$^{-1}$) by dividing with the latent heat of vaporisation $L$ (~2.5 MJ kg$^{-1}$ water).

$H$ and $E$ can also be formulated as functions of the differences in temperature $T$ (°C) and vapor pressure $e$ (kPa) between the surface and the atmosphere:

$$H = \rho_a c_p (T_0 - T_a) f_u \qquad \text{Equation 2-2}$$

$$E = \rho_a \frac{\varepsilon}{p_a} (e_0 - e_a) f_u \qquad \text{Equation 2-3}$$

where $\rho_a$ (kg m$^{-3}$) and $c_p$ (MJ kg$^{-1}$ °C$^{-1}$) are the density and heat capacity of dry air, ε = 0.622 (-) is the ratio of molecular weight of water to dry air, $p_a$ (kPa) is the air pressure. The suffix *0* and *a* represent the surface and the atmosphere, respectively, and $f_u$ (-) is a so-called wind-function representing the efficiency in the turbulent transport of heat and moisture away from the surface.

The first step to eliminate the dependence on the surface conditions is to assume $e_0 = e_s(T_0)$, where $e_s$(T) is the saturation vapour pressure temperature function, and to approximate $e_s(T_0) \approx e_s(T_a) + \Delta(T_0 - T_a)$, where $\Delta$ is the slope of $e_s$(T). This makes it possible to express $E$ as a function of $H$:

$$E = \frac{\varepsilon\Delta}{c_p p_a} H + \frac{\rho_a \varepsilon}{p_a}(e_s(T_a) - e_a) f_u \qquad \text{Equation 2-4}$$

which combined with Equation 2-1 can be written as:

$$E = \frac{\varepsilon\Delta}{c_p p_a}\left(\frac{R_n - G}{L} - E\right) + \frac{\rho_a \varepsilon}{p_a}(e_s(T_a) - e_a) f_u \qquad \text{Equation 2-5}$$

Finally, by introducing the so-called psychrometric "constant" $\gamma = (c_p\, p_a)/(\varepsilon L)$ $(kPa\ °C^{-1})$ and re-arranging Equation 2-5 to eliminate E, the Penman equation for evaporation from open water or a vegetated surface fully supplied with water can be written as:

$$E_{Pen} = \frac{\Delta}{\Delta + \gamma}\frac{(R_n - G)}{L} + \frac{\gamma}{\Delta + \gamma}(e_s(T_a) - e_a) f_u \qquad \text{Equation 2-6}$$

It should be noted that both $R_n$ and $G$ also strongly depends on the surface temperature $T_0$, which means that additional assumptions and approximations are needed to calculate these variables from atmospheric conditions unless provided by observations. Methods to do so are described in Section 2.2.

The following wind functions in unit kg $m^{-2}$ $day^{-1}$ $kPa^{-1}$ were established by Penman (1948, 1956) for open water surfaces:

$$\begin{aligned} f_u &= 2.6(1 + 0.54u_2) \quad \text{Penman(1948)} \\ f_u &= 2.6(0.5 + 0.54u_2) \quad \text{Penman(1956)} \end{aligned} \qquad \text{Equation 2-7}$$

where $u_2$ (m $s^{-1}$) is the wind speed at 2 m elevation above the surface[1]. The first version was established experimentally by Penman (1948), and later corrected theoretically in Penman (1956). According to Halldin (1988), quoting Stigter (1980), Penman considered the original equation more representative for a crop which has higher roughness than an open water surface. The sensitivity to the selection of wind function is evaluated in Section 3.2.1, but in general it depends on the wind speed and on the balance between the first and second main terms in Equation 2-6.

### *Penman equation limitations*

The wind function is probably the main limitation in the Penman-equation, since it has been established empirically based on the data of Penman (1948), without direct relations between its parameters and properties of the vegetation or water surface. It is thus difficult to assess to what degree these are generally valid and possible to transfer or adapt to other conditions. Another problem when applying Penman's equation to a vegetated surface is that its' derivation assumes the surface vapour pressure to be equal to the saturation pressure given by the surface temperature (Monteith 1965). This assumption is probably valid for evaporation of precipitation intercepted on leaves and branches of the vegetation, but not for water inside the leaves (transpiration). Monteith (1965) explains further that, water inside a leaf is evaporating from wet walls inside a stomata cavity, in which the vapour pressure may be close to saturation of the corresponding leaf temperature. However, the vapour is then transported to the surface of the leaf by molecular diffusion, and at the leaf surface, vapour pressure will always be lower than the corresponding saturation pressure given by the leaf surface temperature. This is the background for the concept of a surface resistance controlling the water availability for transpiration, which is a key concept in the Penman-Monteith equations, see Section 2.1.2. In a similar way, the underlying assumption that the available energy for evaporation ($R_n$-$G$) can be estimated independent of the surface conditions is also questionable. Both $R_n$ and $G$ is in reality dependent on the surface temperature that might deviate from the air temperature, especially in cloud-free conditions. On a daily timescale, the errors introduced by this assumption is probably small as argued by Penman

[1] Note that the parameter values in Equation 2-7 are transformed from Penman (1948, 1956) who used miles $day^{-1}$ and mmHg instead of m $s^{-1}$ and kPa as units for wind speed and pressure, respectively.

(1948) – at least with regard to $G$ which typically is much smaller in magnitude than $R_n$ – but may be larger on a sub-daily timescale at which the surface temperature can have a considerable variation and deviation from the air temperature.

### 2.1.2 Penman-Monteith

The Penman-Monteith equation (Monteith 1965) is an extension of the Penman equation, where the empirical wind-function is replaced by a more explicit representation of the surface control on turbulent transport and water availability through the definition of the aerodynamic and surface resistances $r_a$ (s m$^{-1}$) and $r_s$ (s m$^{-1}$), respectively:

$$E_{PM} = \frac{1}{\lambda}\frac{\Delta(R_n - G) + \frac{\rho_a c_p}{r_a}(e_s - e_a)}{\Delta + \gamma\left(1 + \frac{r_s}{r_a}\right)} \qquad \text{Equation 2-8}$$

In addition to the variables already defined in Equation 2-6, Equation 2-8 also contains the density $\rho_a$ (kg m$^{-3}$) and specific heat capacity $c_p$ (MJ kg$^{-1}$ °C$^{-1}$) of dry air. The modifications to Penman's original equation introduced in the Penman-Monteith equation made it possible to relate the surface control to measurable soil and plant physical characteristics such as canopy height, leaf area index, and surface roughness lengths for momentum and heat. In addition, they made it possible to establish plant specific parameters for estimating the surface resistance.

The aerodynamic resistance can be derived from the wind speed, the surface roughness length, and the atmospheric stability using atmospheric boundary layer theory. For transpiration, the surface resistance is related to the stomatal control on the water availability, which, depending on vegetation type, and can be related in various degree to solar radiation, and humidity and temperature in the air. Further, the stomatal control is scaled by the surface area of the transpiring leaves (the leaf area index) – the larger the leaf, the lower the surface resistance. Different models for surface resistance and their implications for practical applications in hydrological modelling are further discussed in Section 2.2.6. The plant control on transpiration will further depend on the soil water availability for root water uptake, as well as on the soil temperature impact on root activity. However, these processes are often added as response functions when estimating ET based on the PET as input.

Conceptually, the Penman (Equation 2-6) and Penman-Monteith equations (Equation 2-8) can be simplified as the sum of two terms, which can be referred to as the 'radiation' and the 'aerodynamic' or 'ventilation' terms. In other words, the equations can be written as the sum of two functions with their corresponding input variables – in the case of Equation 2-8 – net radiation ($R_n$), ground heat flux ($G$), air temperature ($T_a$), actual vapour pressure ($e_a$), wind speed ($u$), and the functions for aerodynamic ($r_a$) and surface resistances ($r_s$):

$$E_{PM} = f_{radiation}(R_n, G) + f_{ventilation}(u, T_a, e_a, r_a, r_s) \qquad \text{Equation 2-9}$$

In this simplified notation, the parameters and functions in Equation 2-8 are lumped into the radiation and ventilation functions $f_{radiation}$ and $f_{ventilation}$. The radiation term would be more accurately defined as the 'available energy' term since it represents $R_n$-$G$, but it is more often referred to as the 'radiation' term in the hydrological literature (e.g. in Allen et al. 1998). Possibly, this is because the net radiation is most often the dominating contribution to the available energy; and in the original derivation of the Penman equation, Penman (1948) even argued that $G$ could be neglected on time scale of a couple to several days. As evident by its name, the ventilation term represents the efficiency in the turbulent transport of moisture from the evaporating surface to the atmosphere, but also the surface control on water availability as already stated above.

### 2.1.3 Other commonly used potential evapotranspiration methods

#### *FAO reference evapotranspiration*

The Food and Agricultural Organization (FAO) reference evapotranspiration – also known as the FAO Penman-Monteith – is an application of the Penman-Monteith equation to a hypothetical reference crop, developed for the United Nations (Allen et al. 1998). The aim was to provide a standardised procedure to estimate reference evaporation for crops consistent with actual crop water use data from

around the world. Parameters were derived based on the assumption of a crop height of 0.12 m, a fixed surface resistance of 70 s $m^{-1}$ and an albedo (fraction of solar radiation reflected by the land surface) of 0.23 corresponding to a green grass field without water limitations. Based on these assumptions and standardised functions for aerodynamic and surface resistances, the FAO Penman-Monteith equation can be written as:

$$E_{FAO} = \frac{0.408\Delta(R_n - G) + \gamma \frac{900}{T_a + 273} u_2 (e_s - e_a)}{\Delta + \gamma(1 + 0.34u_2)} \qquad \text{Equation 2-10}$$

It is further recommended by FAO to use so-called crop coefficients to scale the reference evapotranspiration to potential evapotranspiration for different vegetation types, to consider deviations from the hypothetical crop in terms of the available energy, and aerodynamic and surface resistances. Crop coefficient values for a large variety of agricultural crops and natural surfaces are provided in the FAO crop evapotranspiration guidelines (Allen et al. 1998) available online at https://www.fao.org/3/x0490e/x0490e00.htm. Values are given as a function of crop growth development, typically with lower values well below 1 in the early stage of development, peak values between 1 and 1.25 (sugar canes), and somewhat lower than the peak values towards the end of the growth period. For conifer forests, FAO suggest a crop coefficient equal to 1, with a remark that it may be considerably lower since conifers typically have a strong stomata control to compensate for low aerodynamic resistances (tall vegetation creates more turbulence in the air, which enhances the moisture transport away from the surface).

### *Priestley-Taylor*

Priestley and Taylor (1972) found that evaporation from saturated surfaces could be described by the following equation:

$$E_{PT} = \alpha \frac{\Delta}{\Delta + \gamma}(R_n - G) \qquad \text{Equation 2-11}$$

where $\alpha$ is an empirical parameter which was estimated by Priestley and Taylor (1972) to 1.26 through analyses of several datasets over ocean and land. The Priestley-Taylor equation is essentially identical to the first term in the Penman (1948) equation (Equation 2-6), suggesting that the potential evapotranspiration is linearly related to the available energy and, thereby, neglecting the impact of atmospheric humidity and ventilation by the wind. It has subsequently been found that the Priestley-Taylor equation is more suitable for applications in humid climates rather than in arid climates (Oudin et al. 2005).

### *Jensen-Haise McGuiness*

The 'Jensen-Haise McGuiness' equation was found to be the overall best performing PET-equation in a large inter-comparison study (Oudin et al. 2005), where 27 different PET-equations were implemented in a hydrological model calibrated to observed runoff for over 300 river basins in France, Australia and the United States. It is an air temperature index model with a latitude-dependent seasonal variability. It was originally suggested by Jensen and Haise (1963) and later modified by McGuiness and Bordne (1972) to:

$$E_{JHM} = \begin{cases} \frac{R_e}{\lambda\rho} \frac{T_a + 5}{100} & if\ T_a + 5 > 0 \\ 0 & otherwise \end{cases} \qquad \text{Equation 2-12}$$

where $R_e$ (MJ $m^{-2}$ $day^{-2}$) is the extra-terrestrial solar radiation, which is a function of latitude and day of the year, λ is the latent heat of vaporization (MJ $kg^{-1}$), ρ is the density of water (kg $m^{-3}$) and $T_a$ is the air temperature (°C). The empirical parameters 5 and 100 were proposed by Oudin et al. (2005).

***Temperature index with seasonal delay from the HYPE model***

Rohde et al. (2006) developed a temperature-based function for potential evapotranspiration, which was later implemented in the hydrological model HYPE (Lindström et al. 2010):

$$E_{HYPE} = \begin{cases} C_e T_a B(t) & if\ T_a > 0 \\ 0 & otherwise \end{cases}$$
$$B(t) = (1 + Asin(2\pi \frac{t+\psi}{365} - \frac{\pi}{2})$$

Equation 2-13

where $C_e$ (mm °C$^{-1}$ day$^{-1}$) is a temperature index coefficient, $T_a$ (°C) air temperature, and $B(t)$ a sinusoidal function of the day of the year $t$ (1 to 365), which can be used to generate a seasonal delay in the evaporation temperature response. In the latter, $A$ is the amplitude and $\psi$ is a phase shift factor (days). The $E_{HYPE}$ function has been calibrated for different land cover types in Sweden as part of the S-HYPE model (Strömqvist et al. 2012) which is used by SMHI for the national water resource monitoring and flood forecasting in Sweden. In the current version of the S-HYPE model (SHYPE2016f), the amplitude and phase shift parameters are set to 0.27 and 67.5 respectively, and the median value of the land-use dependent $C_e$ parameters is set to 0.131.

### 2.1.4 Dual-source potential evapotranspiration models

The PET models presented in Sections 2.1.1 to 2.1.3 can all be classified as 'single-source' models, meaning that these models consider the land surface as one evaporating surface for which the PET is representative. To calculate ET from different evaporation components using the PET concept, there are essentially two alternatives as illustrated in Figure 2-1:

1) to estimate PET with a single set of input conditions, which is subsequently distributed to provide PET for the different sub-components with some distribution function, or
2) to distribute the input conditions to the different sub-surfaces and apply appropriate PET functions separately for each component.

The main advantage of the second 'multi-source' option is that it makes it possible to select different PET functions and/or response functions for the different evaporation components to better reflect their characteristics and responses to the physical conditions.

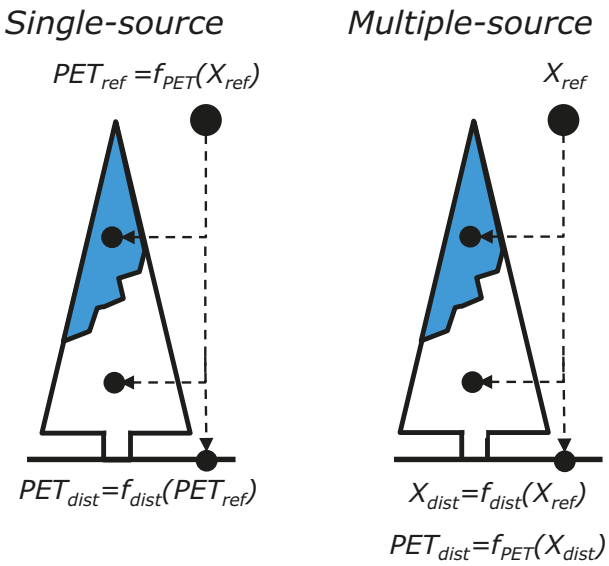


***Figure 2-1.*** *Conceptual diagram to illustrate the difference between a single-source and a multiple-source PET model for estimating PET for transpiration as well as soil and canopy evaporation; in the single-source model, PET is estimated as a function of a single set of input conditions $X_{ref}$ and subsequently partitioned with some function $f_{dist}$ to obtain PET for the evaporation components. In the multiple-source model, the input conditions are first distributed to the different sub-surfaces, and subsequently used as input to PET functions applied for the sub-components separately.*

In a boreal terrestrial ecosystem, the most important evaporating components are the transpiration, soil evaporation and canopy evaporation. Since transpiration and canopy evaporation originates from the same 'surface' exposed to the same conditions with regard to the available energy and transport efficiency away from the surface, a dual-source model, representing evaporation from a vegetation layer and a ground layer below is the most common approach implemented in hydrological and meteorological models (e.g. Deardorff 1978, Shuttleworth and Wallace 1985, Blyth et al. 1999, Gustafsson et al. 2004). However, if the functions to distribute the input conditions to more than two layers are available, most of these models can be extended to multiple-sources. The methods for distribution of the input conditions (e.g. net radiation, ground heat flux, and aerodynamic resistances) are presented in Section 2.2.

The most important characteristic for distribution of the input conditions is probably the density of the vegetation represented by the leaf area index (LAI), which governs the transmission of radiation through the canopy layer. The transmission of radiation through a canopy can be relatively well represented by an exponential function called Beer's Law ($R_{canopy} = R_{above}\,(1-e^{-k\,LAI})$, and $R_{ground} = R_{above}\,e^{-k\,LAI}$), and will be used in Section 2.2 both in the estimation of effective albedo, and distribution of net radiation for the dual-source model. The same principle may be used for single-source models to distribute the common PET between the components ($PET_{canopy} = PET_{ref}\,(1-e^{-k\,LAI})$ and $PET_{ground} = PET_{ref}\,e^{-k\,LAI}$) as was shown e.g. by Hansen (1984).

In a dual-source model, the separation between transpiration and canopy evaporation is relatively straight forward: the aerodynamic resistance can be assumed identical, the surface resistance for canopy evaporation can be assumed to be zero (and it should anyway be estimated for transpiration), and the available energy can be partitioned as a function of the fraction of the vegetation covered by intercepted water. In a single-source model, this is less straight forward and depend on how the reference PET is defined.

## 2.2 Input data requirements

Following FAO (Allen et al. 1998), the factors controlling evapotranspiration can be sorted into 3 groups: (i) meteorological, (ii) vegetation and (iii) management and environmental conditions. The PET functions described in the previous section represent these conditions through the input variables and parameters, and by how these are combined. The meteorological conditions include many of the input variables, such as air temperature, wind speed, humidity, net radiation and ground heat flux. These variables correspond to atmospheric and surface conditions that have a direct impact on the available energy for evapotranspiration and/or the vapour transport efficiency. Additional meteorological variables that are useful include snow depth and cloudiness. The vegetation conditions are represented by inputs such as the leaf surface resistance and the fraction of solar radiation reflection (surface albedo), which have an impact on the availability of water and the available energy, respectively. The vegetation conditions are typically dependent on the type of vegetation and the time of year, and to some extent also controlled by the meteorological conditions. The management and environmental conditions are more related to the transformation from potential to actual evapotranspiration – for example the soil water content – and will not be further discussed in this report.

In the following sub-sections, the input variables and methods to obtain these variables are discussed in more detail. An overview of the required input variables is presented in Appendix A, Table A-1, where they are further categorised depending on the usage in the PET calculation, and the typical (or primary) data source.

### 2.2.1 Air temperature, air humidity, and related atmospheric variables

**Air temperature ($T_a$)** is a key input variable used indirectly or directly in all the methods for potential evapotranspiration included in this study (Equations 2-6, 2-8, 2-10, 2-11, 2-12, and 2-13) and most often provided as part of the meteorological input data. Although not directly used in the Penman, Penman-Monteith and Priestley-Taylor equations (Equations 2-6, 2-8, 2-10, and 2-11), air temperature is a key input variable to several of the sub-functions embedded in these equations,

for instance the saturated vapour pressure ($e_s$) and its slope ($\Delta$), the psychrometer constant ($\gamma$), as well as for approximation of the net radiation and ground-heat flux unless these are available from observations. The latent heat of vaporization ($\lambda$) is also a function of air temperature, but the effect is small and sometimes neglected.

**Actual vapour pressure ($e_a$)** is another key input variable to the Penman-type of equations. It can be calculated from relative humidity ($RH$) and the saturation vapour pressure temperature function. Actual vapour pressure is also an important factor for estimating the thermal radiation from the atmosphere, which is included in the net radiation (see Section 2.2.2). Air humidity is further known to be one of several controlling factors regulating the canopy surface resistance to transpiration (see Section 2.2.5). Depending on surface resistance function, air humidity may be needed in the form of specific humidity ($q$), relative humidity or actual vapour pressure. Transformation from vapour pressure to specific humidity further requires the air pressure ($p_a$). Equations to derive $e_s$, $e_a$, $q$, $\Delta$, $\gamma$ and $\lambda$ based on air temperature, relative humidity and air pressure are given in Appendix A, Sections A2.1 to A2.6. If air pressure is not available, a constant pressure of 101.3 kPa is typically assumed.

### 2.2.2 Net radiation

**Net radiation ($R_n$)** is the net sum of upward and downward shortwave and longwave radiation components:

$$R_n = R_s(1 - \alpha) + R_{L,down} - R_{L,up} \qquad \text{Equation 2-14}$$

where $R_s$ is the downward shortwave radiation at the land surface (also known as global radiation), $\alpha$ is the albedo, which is the fraction of $R_s$ reflected by the land surface, and $R_{L,down}$ and $R_{L,up}$ is the downward and upward longwave (thermal) radiation emitted by the atmosphere and the land surface respectively. Throughout the report, the unit for net radiation and its components is MJ $m^{-2}$ $d^{-1}$ if not stated otherwise.

If observations of shortwave and longwave radiation components are not included in the meteorological data, they can be estimated from other available information and data. The FAO guidelines (Allen et al. 1998) provide equations and detailed workflows for estimation of missing radiation data depending on data availability, local conditions and level of accuracy needed. Eriksson (1981) applied similar but not identical methods including adjustments to Swedish conditions. The deviations between Eriksson (1981) and FAO with regard to radiation estimation is described in more detail in the workflow below, and in Appendix A, Section A2.

If global radiation ($R_s$) is available, as in the SKB measurements at Forsmark, the recommended workflow to estimate net radiation ($R_n$) can be summarised with the following calculation steps:

1. **Extra-terrestrial radiation ($R_{ext}$)** – the shortwave radiation outside the atmosphere projected per unit area of the ground – calculated as a function of latitude, day of the year, solar declination and solar constant (see Appendix A, Section A2.7).
2. **Cloudiness** and **Atmospheric turbidity** – turbidity is the ratio of the global radiation to the extra-terrestrial radiation ($\tau = R_s/R_{ext}$), and is strongly related to cloudiness, which is the fraction of the sky covered by clouds. In order to estimate cloudiness from the global radiation, a model for the turbidity at clear-sky conditions and 100 % overcast conditions need to be selected. FAO recommends a simple linear relationship between a maximum turbidity of 0.75 at clear sky and 0.25 at full cloud cover, whereas Eriksson (1981) used a seasonal variation in the maximum and minimum turbidity, with one set of values for summer and one for winter. FAO further recommend turbidity formulas considering the angle of the sun above the horizon for high latitudes and low solar angles. The impact of the selection of these three turbidity models is further examined in this report. Details about the turbidity models and their application are given in Appendix A, Section A2.8.
3. **Clear-sky radiation ($R_{so}$)** – is the global radiation at cloud-free conditions, and can be calculated from the extra-terrestrial radiation and the maximum atmospheric turbidity according to the chosen model, see discussion in the previous step and Appendix A, Section A2.8.
4. **Relative shortwave radiation ($R_s/R_{so}$)** – is calculated as the ratio of the global radiation and the clear sky radiation. It is a different characteristic compared to the turbidity and cloudiness indices, and is used in the estimation of net longwave radiation as described further down.

5. **Snow depth and albedo of snow-covered ground** – presence of snow on the ground (and on the vegetation) has a large impact on the reflection of shortwave radiation, which is totally neglected by FAO. Eriksson (1981) as well as Penman-SMHI used observed snow depth at nearby stations to switch between a snow-free albedo of 0.12 and albedo of snow-covered ground of 0.50. To further improve the estimates of snow and snow albedo, a simple degree day model for the snow pack evolution as a function of air temperature and precipitation was applied. The snow/rain threshold and degree day melt coefficients were adopted from Johansson and Öhman (2008) who estimated these parameters using the snow observations in open and forest areas in Forsmark. Details on the snow modelling are provided in Appendix A, Section A3.
6. **Albedo (α) and Net shortwave radiation ($R_{sn}$)** – albedo is the fraction of global radiation reflected by the land surface and is an essential variable to calculate the shortwave radiation absorbed by the land surface. The FAO reference evapotranspiration method is using a constant albedo of 0.23, which is relevant for agricultural crops and short cut grass. Natural grassland and forests usually have lower albedo of around 0.1, whereas snow surfaces can have albedo in the range between 0.4 (old snow) and 0.9 (fresh snow). The albedo of snow-covered ground is discussed in the previous step. For a dual-source evapotranspiration framework, considering the distribution of radiation between a vegetation (canopy) layer and the underlying ground, an effective albedo of the land surface can be defined using the so-called 'Beer's Law':

   $$\alpha_{effective} = (1 - e^{-k_{lai}LAI})\alpha_{canopy} + e^{-k_{lai}LAI}\alpha_{ground}$$ Equation 2-15

   where LAI is the leaf area index ($m^2\ m^{-2}$) of the vegetation layer, and $k_{lai}$ is an exponential extinction coefficient with values typically found around 0.6 (Rasmus et al. 2013, Stähli et al. 2009). Estimates of leaf area index and albedo for different types of boreal land surface types are discussed in more detail in Section 2.3.3.

   Once the land surface albedo is calculated based on the FAO, Eriksson (1981) or the dual-source model presented in this report, it is straight forward to derive the net shortwave radiation as:

   $$R_{sn} = (1 - \alpha)R_s$$ Equation 2-16

7. **Net longwave radiation ($R_{ln}$)** – Instead of calculating the downward and upward longwave radiation components separately, which would require an estimate of the land surface temperature, FAO as well as Eriksson (1981) used a single formula to derive the net longwave emission ($R_{ln} = R_{L,up} - R_{L,down}$) directly based on the formula suggested by Brunt (1932):

   $$R_{ln} = \sigma(T_a + 273.15)^4\left(b_1 - b_2\sqrt{e_a}\right)\left(b_3 + b_4\frac{R_s}{R_{so}}\right)$$ Equation 2-17

   where $\sigma$ is the Stofan-Boltzmann constant ($4.903 \times 10^{-9}$ MJ $K^{-4}$ $m^{-2}$ $d^{-1}$), $e_a$ is the actual vapour pressure (kPa), $R_s/R_{so}$ is the relative shortwave radiation (-) and $b_1 = 0.34$, $b_2 = 0.14$ $kPa^{-0.5}$, $b_3 = -0.35$, and $b_4 = 1.35$ are empirical constants with values as suggested by FAO ($b_1$, $b_3$, and $b_4$ are unitless while $b_2$ has the unit $kPa^{-0.5}$). Eriksson (1981) used a slightly different implementation of the Brunt equation, where $e_a$ is given in mb instead of kPa, and cloudiness (-) is used instead of relative shortwave radiation. He also used different parameter values; $b_1 = 0.56$, $b_2 = 0.08$ $mb^{-0.5}$, $b_3 = 1$, and $b_4 = -0.9$. The use of $b_2 = 0.08$ $mb^{-0.5}$ is equivalent to $b_2 = 0.25$ $kPa^{-0.5}$, which is similar to the value suggested in an earlier version of the FAO guidelines (Doorenbos and Pruitt 1977). The use of cloudiness instead of relative solar radiation explains the different signs and magnitudes in $b_3$ and $b_4$. However, it should be noted that cloudiness varies between 0 and 1, and the relative shortwave radiation varies between around 0.3 and 1 depending on the turbidity model. These slight differences in the implementations of the Brunt formula do have a substantial impact on the estimated net longwave radiation, which is further analysed in Section 3.1.2. In addition to the FAO and Eriksson versions, the Brunt parameters where calibrated using the upward and downward radiation data from the ICOS stations in Norunda and Svartberget to produce the best possible estimate of net longwave radiation for the study areas.

8. **Net radiation ($R_n$)** – the final step is to calculate net radiation as the net (downward) shortwave radiation minus the net (upward) longwave radiation:

$$R_n = R_{sn} - R_{ln} \quad \text{Equation 2-18}$$

For a dual-source evapotranspiration framework, the total net radiation can thus be distributed between the canopy layer and the ground below using a similar equation as used to estimate the effective albedo:

$$R_{n,canopy} = \left(1 - e^{-k_{lai}LAI}\right)R_n$$
$$R_{n,ground} = e^{-k_{lai}LAI}R_n \quad \text{Equation 2-19}$$

### 2.4.3 Ground heat flux

**Ground heat flux (G)** is not commonly available from meteorological observation systems. When measured at research sites such as the ICOS sites in Krycklan/Svartberget and Norunda, it often represents the vertical heat flux in the top soil layer. However, this is not necessarily representative for the heat storage heat flux related to e.g. the evaporative surfaces for transpiration or sublimation of snow on the ground. *G* should ideally be observed or calculated separately for each evaporating surface within the land surface (the vegetation canopy, the snow and/or bare soil surface, the open water), but is often assumed to be zero or approximated with relatively simplified models.

The most commonly used methods for estimating ground heat flux for PET estimation are either based on the net radiation and/or air or surface temperature data as reviewed by Purdy et al. (2016), who made an inter-comparison of 6 different ground heat flux methods. For the Penman-SMHI calculations, the method of Gardelin and Lindström (1997) which is only dependent on the net radiation was used. Similar types of methods were included in the review by Purdy et al. (2016), which concluded that it is not possible to single-out one particular method that was generally better than the others. For simplicity, the Gardelin and Lindström (1997) method is also used in this study. However, it is further developed using two scaling parameters to allow for calibration of the relation to negative and positive net radiation values separately:

$$G = \begin{cases} g_{pos}(-10 + 0.22R_n) & if\ R_n \geq 0 \\ g_{neg}(-10 + 0.22R_n) & if\ R_n < 0 \end{cases} \quad \text{Equation 2-20}$$

where $G$ and $R_n$ are given in units W m$^{-2}$.

The overall impact of insulation of the soil by vegetation and snow, and the variation of soil thermal conductivity due to soil moisture and freezing is difficult to predict, which is why two separate scaling factors were introduced for the calibration of the Gardelin and Lindström (1997) equation. It should also be noted that snow also affects the heat capacity of the land surface, which may increase the ground heat flux, especially during the snow melt period. The scaling factors were calibrated using the ground heat flux data available from Krycklan/Svartberget and Norunda, and the results of the calibration is discussed in Chapter 3.

The ground heat flux method presented here is not suitable for estimating the available energy for evaporation over open water with water depths larger than 1 m as recommended by Finch and Hall (2001). They further recommend the equilibrium temperature method based on the work of Edinger et al. (1968) as a superior model for lake evaporation compared to the Penman-Monteith or Penman equations. Lake evaporation will not be further discussed in this report, which focus on evapotranspiration from land surfaces.

### 2.4.4 Wind speed

Wind speed is usually measured at 10 m above the ground, as opposed to other meteorological variables which are measured at 2 m height. This means that the wind speed needs to be transformed to represent the same height as the other variables. The recommended model for the wind speed

transformation to the common reference height is through the logarithmic wind profile, which relates the wind ($u_z$) at the height $z$ above the surface to the so-called friction velocity ($u_*$) through:

$$u_z = \frac{u_*}{k} log\left(\frac{z-d}{z_{0m}}\right) \quad \text{Equation 2-21}$$

where $k$ is the Karman constant (0.41), $d$ is the zero-plane displacement height, and $z_{0m}$ is the surface roughness length for momentum transfer. Transformation from 10 m wind to 2 m wind can thus be made through:

$$u_{2m} = u_{10m} log\left(\frac{2-d}{z_{0m}}\right) / log\left(\frac{10-d}{z_{0m}}\right) \quad \text{Equation 2-22}$$

The roughness length for momentum transfer is approximately 10 % of the height of the structures on the land surface, that is the height of the vegetation in this context. However, it may vary due to the shape and density of the canopy foliage. The zero-plane displacement height can be further estimated to about 2/3 of the height of the vegetation. The FAO reference evapotranspiration equations was developed for a hypothetical canopy with height 0.12 m and roughness length derived as a fraction 0.123 of the canopy height ($z_{0m}$ = 0.123 × 0.12 = 0.015) and $d$ = 0 (Allen et al. 1998). The fraction 0.123 corresponds to 1/8 of the canopy height compared to the standard value 1/10. These parameters generate a windspeed transformation factor $u_{2m}/u_{10m}$ = 0.75. In comparison, the procedure followed to calculate the Penman-SMHI dataset used $u_{2m}/u_{10m}$ = 0.8. In the revised procedure used in this study, $z_{0m}$ and $d$ were derived from canopy heights separately for each vegetation type, using the factors 0.123 and 2/3, respectively, in line with the FAO guidelines. Canopy heights for different vegetation types were extracted from a global database of land surface characteristics called ECOCLIMAP-SG (Masson et al. 2003, CNRM 2018, Druel et al. 2022). This database is described in more detail in Section 2.3.3.

For application of the Penman-Monteith equation to forested areas, there is a need to transform the measured windspeed to a representative height above the forest canopy. Transformation of wind speed from one height to another is a straightforward task using Equation 2-22 as long as the windspeed is measured above the same vegetation stand as we want to transform it for. However, transformation of windspeed measured above a low vegetation to some height above a tall vegetation is less trivial, since we cannot assume the friction velocity to be the same above the two types of vegetation.

Silversides (1978) estimated the relation between windspeed measured at airports and the windspeed over forests assuming the two areas being subject to the same geostrophic wind. Depending on the canopy heights as well as estimates of roughness lengths and displacement heights, his results suggest that the ratio in the windspeed between an open-field and 10 m above the forest canopy height is within the range 0.4 to 0.7. However, airports are typically located in windy large open areas that might not be representative for the locations of a typical weather station in a boreal forest landscape. Such stations are more likely located on smaller open areas surrounded by forest stands much closer than at an airport. Since this is the situation for the data used in this study, the following assumption is made:

- *the wind speed measured at (or transformed to) 10 m above the zero-plane displacement height at the measurement site is representative for the wind speed at 10 m above the zero-plane displacement height at any site located within the area exposed to the same general wind-field as the measurement site.*

This assumption was tested using the wind speed measurements at 36 and 34 m height above the forests at the Norunda and Krycklan/Svartberget study areas, respectively, and windspeed data from a selection of surrounding SMHI weather stations for both locations, where wind speed is measured at 10 m height in open terrain (see Section 2.3). The windspeed from the surrounding weather stations ($u_{10m,station}$) were transformed to windspeed ($u_{zlocal}$) at the local measurement heights ($z_{local}$) by applying Equation 2-22 as:

$$u_{Zlocal} = u_{10m,station} log\left(\frac{z_{local}-d_{local}}{z_{0m,local}}\right) / log\left(\frac{(d_{local}+10)-d_{local}}{z_{0m,local}}\right) \quad \text{Equation 2-23}$$

### 2.4.5 Aerodynamic resistances in single and dual-source evapotranspiration models

#### *Standard formulation for a single-source evaporating surface*

The standard equation to calculate the aerodynamic resistance $r_a$ (s m$^{-1}$) for heat and water vapour flow from an evaporating surface to the air can be found in many publications, as for instance in the FAO guidelines (Allen et al. 1998). In the following equation, the aerodynamic resistance is formulated for a surface with roughness lengths for momentum exchange $z_{0m}$, roughness length for heat and water vapour exchange $z_{0h}$, and displacement height $d$:

$$r_a = \frac{log\left(\frac{z_{ref} - d}{z_{0m}}\right) log\left(\frac{z_{ref} - d}{z_{0h}}\right)}{k^2 u_z} \qquad \text{Equation 2-24}$$

where $k$ is the Karman constant (0.41) and $u_z$ is the wind speed at the common reference height $z_{ref}$ for the windspeed, temperature and water vapour measurements. It should be noted that Equation 2-24 is valid for neutral conditions with regard to the atmospheric stability. Neutral conditions means that there are no vertical temperature gradients that would otherwise enhance (unstable) or reduce (stable) the turbulent vertical transport of momentum (or moisture). Equation 2-24 can thus be further generalised to be more accurate for unstable and stable conditions by addition of so-called stability correction functions for momentum and heat, respectively. However, estimating the atmospheric stability requires knowledge about the surface temperature, or more precisely the direction of the vertical temperature gradient in the atmospheric surface layer, which is omitted due to the assumptions underlying the Penman and Penman-Monteith equations. Allen et al. (1998) further argues that stability corrections might be needed only at hourly or shorter time-scales, and that the well-watered surface conditions for which the potential evapotranspiration is defined should be more representative for neutral conditions.

As stated in the previous section, the roughness length for momentum can be estimated with about 1/10 of the height of the roughness elements, which for a vegetated surface means 1/10 of the canopy height. Following the FAO guidelines, a slightly higher fraction corresponding to ~1/8 is used so that $z_{0m}$ is calculated here as 0.123 times the canopy heights of the different vegetation types considered. Furthermore, the roughness length of heat and water vapour exchange is typically estimated to be around 1/10 of the roughness length for momentum, which is also used in this study.

#### *Aerodynamic resistances for evaporation from a dual-source ground-vegetation system*

The standard formulation of the Penman and Penman-Monteith equations estimates PET from one single evaporating surface. Depending on the formulation of the available energy and surface resistance, the equation can be assumed to be representative for one or a combination of several evaporating surfaces existing in a system – for instance the transpiration from the tree layer, if the system is a forest. It is also possible to define a dual-source system, where the available energy, and aerodynamic and surface resistances are estimated separately for a vegetation layer and a ground layer below, to enable the application of the Penman-Monteith equation separately for the two layers.

The distribution of net radiation between a vegetation layer and the ground layer is described in Section 2.2.4. For a daily time-step, it is safe to assume that the ground heat flux can be neglected for the vegetation layer, and thus let the available energy for the vegetation and ground layers be defined by:

$$\begin{aligned}(R_n - G)_{canopy} &= R_{n,canopy} - 0 \\ (R_n - G)_{ground} &= R_{n,ground} - G\end{aligned} \qquad \text{Equation 2-25}$$

where $R_{n,canopy}$ and $R_{n,ground}$ are given by Equation 2-19 and $G$ is given by Equation 2-20.

Following Blyth et al. (1999), the aerodynamic resistances for a dual-source system are constructed by defining excess resistances from the canopy surface to the canopy air ($r_{ac}$), and from the ground surface to the canopy air ($r_{ag}$), in addition to the aerodynamic resistance between the canopy air to the reference height above the canopy ($r_{aa}$):

$$\begin{aligned}r_{a,canopy} &= r_{aa} + r_{ac} \\ r_{a,ground} &= r_{aa} + r_{ag}\end{aligned} \qquad \text{Equation 2-26}$$

The resistance from the canopy air to the reference height is calculated using Equation 2-24 with effective displacement heights ($d$) and roughness lengths ($z_{0m}$ and $z_{0h}$) calculated with snow depth correction (not shown in detail here) following Bewley et al. (2010).

Following Blyth et al. (1999), the excess resistances are defined by the roughness lengths for heat transfer for the canopy ($z_{0hc}$) and ground ($z_{0hg}$) layers, respectively:

$$r_{ac} = \frac{log((d - z_{0h})/z_{0hc})}{u_* k}$$
$$r_{ag} = \frac{log\big((d - z_{0h})/z_{0hg}\big)}{u_* k}$$

Equation 2-27

where $u_*$ and k are the friction velocity and Karman constant as defined in Equation 2-21 and the roughness lengths for heat transfer are derived as 1/10 of the corresponding roughness lengths for momentum following the same principle as discussed above. For sparse to closed vegetation, $r_{ag}$ can be further adjusted as a function of the fractional canopy cover ($f_c$) following Menard et al. (2014):

$$r_{agc} = \frac{1}{\big((1 - f_c)/r_{ag} + f_c u_* C_0\big)}$$

Equation 2-28

where $C_0$ is a constant sub-canopy heat exchange rate for 100 % canopy cover given a value of 0.004 by Menard et al. (2014).

### 2.4.6 Surface resistance

The surface resistance $r_s$ (s m$^{-1}$) characterises the control of the evaporating surface on the water availability as defined in the Penman-Monteith equation (Equation 2-8). For transpiration, this control has been found to be related to various atmospheric and soil conditions, such as the level of solar radiation, temperature and humidity in the air, as well as the temperature and moisture content of the root zone of the soil. It has also been found to scale linearly as a function of the leaf areas. The impact of the soil conditions is typically not considered when calculating PET, since it would require to include these variables in the input data. Typically, the soil conditions are instead used to calculate the actual ET from the PET as part of a hydrological or land-surface model.

By defining a minimum surface resistance per leaf area index, $r_{smin}$ (s m$^{-1}$), and a general response function $f(x)$ where $x$ represents the various environmental conditions considered and $f(x)$ varies between 1 (favourable conditions) and 0 (non-favourable conditions), the bulk surface resistance can be formulated as:

$$r_s = \frac{r_{smin}}{LAI\ f(x)}$$

Equation 2-29

When $f(x)$ changes from 1 to 0, $r_s$ increases from $r_{smin}/LAI$ towards infinity.

The surface resistance used for the FAO reference evapotranspiration (Allen et al. 1998) is based on a minimum surface resistance of 100 s m$^{-1}$ and an active (sunlit) leaf area index of 1.44, which gives a bulk surface resistance of about 70 s m$^{-1}$.

To improve the surface resistance calculations for the vegetation types found in boreal forests, the surface resistance model used in the land surface model SURFEX (Le Moigne 2018) is used with input parameters extracted for the study areas from the ECOCLIMAP-SG database (see further Section 2.3.3). The surface resistance formulation in SURFEX follows the general formulation (Equation 2-29) with multiplicative response functions for global radiation ($F_R$), specific humidity deficit ($F_q$), air temperature ($F_T$), and soil moisture ($F_S$) are defined as:

$$f(x) = F_R F_q F_T F_S$$

Equation 2-30

and the radiation, humidity and temperature functions are given by:

$$F_R = \frac{f_R + r_{smin}/r_{smax}}{1 + f_R} \qquad \text{Equation 2-31}$$

$$f_R = 0.55 \frac{R_s}{RGL} \frac{2}{LAI}$$

$$F_q = 1 - \gamma(q_s - q_a) \qquad \text{Equation 2-32}$$

$$F_T = 1 - 0.0016(T_{a,K} - 298.15)^2 \qquad \text{Equation 2-33}$$

where *RGL* and *y* are vegetation-type specific parameters for the radiation and air humidity response extracted from the ECOCLIMAP-SG database (Section 2.3.3). The other parameters in Equations 2-31 to 2-33 are $r_{smax}$ (s m$^{-1}$) a maximum allowed aerodynamic resistance here set to 5 000 s m$^{-1}$, $R_s$ (W m$^{-2}$) the global radiation, $q_s$ (kg kg$^{-1}$) and $q_a$ (kg kg$^{-1}$) are the saturated and actual specific humidity in the air (see Appendix 1), and $T_{a,K}$ (K) is the air temperature in Kelvin. The soil moisture response function is set to 1 to obtain a surface resistance relevant for the definition of PET used in this report.

For evaporation from open water and from precipitation intercepted on the vegetation, the surface resistance is typically set to 0, and for the soil evaporation, the surface resistance can be approximated by a constant or a function of the soil surface moisture content. For this study, the soil surface resistance is assumed to be equal to the bulk surface resistance used for the FAO reference evapotranspiration (70 s m$^{-1}$).

### 2.4.7 Leaf area index

Leaf area index (LAI, m$^2$ leaf per m$^2$ ground) is one of the most important vegetation characteristic influencing evapotranspiration as well as the land surface energy balance in general and the carbon turnover. Lindroth et al. (2008) showed that the variation in LAI is the most important variable to explain the differences for both photosynthesis and respiration between a large sample of northern coniferous and deciduous forest sites.

LAI controls the transmission of solar and thermal radiation through the canopy layer as described in Section 2.2.2, where the exponential 'Beer's Law' is used both for estimating the effective albedo of a vegetated land-surface, and for distributing the net radiation between canopy and ground layers. The former is most important during winter, when the albedo of the ground layer (snow) is much higher than the albedo of the canopy layer (unless this is also covered by snow).

LAI can also be related to the canopy closure or openness, which in turn also is related to transmission of direct solar radiation as well as direct throughfall of precipitation. Rasmus et al. (2013) investigated the sensitivity of snow interception and mass balance modelling to the definitions and estimations of LAI, canopy coverage ($C_c$) and sky-view fraction $F_{sw} = (1-C_c)$. The equation suggested by Verseghy et al. (1993):

$$F_{sv} = e^{-0.5LAI} \qquad \text{Equation 2-34}$$

is similar in form to Equation 2-19 and was found to give best results when assessed with LAI and sky view fractions estimated optical observations over 7 boreal forest sites in Sweden and Finland (Rasmus et al. 2013).

LAI also provides storage capacity for intercepted precipitation and, most importantly, for evapotranspiration modelling it provides scaling of the stomata resistance; it is used directly in the surface resistance models described in Section 2.2.6.

There exist several satellite-based global LAI products, for instance by the EU Copernicus global land monitoring services https://land.copernicus.eu/global/products/lai. The leaf area index data in this study is extracted from the ECOCLIMAP-SG database (Section 2.3.3), which in turn is based on the same satellite data as the Copernicus service.

## 2.3 Study areas and data

### 2.3.1 Forsmark

Forsmark is located on the east coast of Sweden at latitude/longitude 60° 22' N, 18° 11' E. Located in the boreal zone, the investigated area potentially affected by the planned repository for spent nuclear fuel and the existing repository for short-lived radioactive waste (SFR), is covered by conifer forests dominated by Scots Pine and Norway Spruce, mixed forest with broadleaf species such as birch and aspen, and due to the low topographical relief, also a significant fraction of wetlands and shallow lakes. There is also agricultural land, as well as build-up areas. Detailed information on the hydro-geological, climatological and vegetation characteristics of the area can be found in Löfgren (2010). A comprehensive investigation and monitoring program have been conducted by SKB including relevant hydrological, meteorological, geological and ecological parameters as described in Werner et al. (2013, 2014). For this study, a selection of meteorological observations from Forsmark was used covering the years 2003–2016, as summarised in Table 2-1:

**Table 2-1. Meteorological data from Forsmark used in the study.**

| Variable | Time resolution | Height | Location/comment | Data source |
|---|---|---|---|---|
| *Inputs to the potential evapotransporation calculations* | | | | |
| Air temperature | 30 min | 2 m | Forsmark (Högmasten, Storskäret) | SKB |
| Air temperature | daily | 2 m | Forsmark, aggregated, gap-filled | SKB |
| Relative humidity | 30 min | 2 m | Forsmark (Högmasten, Storskäret) | SKB |
| Wind speed | 30 min | 10 m | Forsmark (Högmasten, Storskäret) | SKB |
| Global radiation | 30 min | 2 m | Forsmark (Högmasten) | SKB |
| Precipitation | daily | 2 m | Forsmark, aggregated, corrected, gap-filled | SKB |
| *Data for calibration and evaluation* | | | | |
| Potential evapotranspiration | 30 min | | Forsmark (Högmasten, Storskäret), derived by SMHI[1] | SKB |
| Potential evapotranspiration | daily | | Forsmark, aggregated, gap-filled | SKB |
| Cloudiness | hourly | | Films, Örskär | SMHI |
| Snow depth and snow water equivalent | daily | | Forsmark (at Storskäret, representing open land, and at Bolundsfjärden and Jungfruholm representing forest) | SKB |

[1] Calculated with the Penman-SMHI function following Eriksson (1981).

Continuous time series of daily mean precipitation corrected for measurement errors, air temperature and potential evapotranspiration (Penman-SMHI following Eriksson (1981)) were provided by SKB. Additional daily values for minimum and maximum air temperature, wind speed, relative humidity, and global radiation were derived from the original 30-minute data provided by SKB, complemented with hourly data on air temperature, humidity and windspeed from the surrounding SMHI weather stations in Films and Örskär (windspeed only), and global radiation from the SMHI solar radiation re-analysis model STRÅNG (http://strang.smhi.se) for gap-filling.

For each variable, a single time-series with 30-minute data was first created by combining data from the 4 SKB weather stations in Forsmark, using data from the different stations in the following priority: PFM010700_001, PFM010700_002, PFM010701 and PFM006281. The remaining gaps were filled with data primarily from Films (or STRÅNG in the case of global radiation) with the following procedure: in a first step, the hourly data from the SMHI stations were matched with the SKB data on the full hour for overlapping data periods, in order to derive linear regression relationship that was subsequently used to predict the missing data at the full hour in the Forsmark time-series. Secondly, the missing data at the full hour plus 30 minutes were filled by linear interpolation between the surrounding values at the full hour. For windspeed, it was found that the Örskär station provided data with higher correlation to the Forsmark data, and was thus used for the gap-filling instead of the data from Films. For the global radiation, the data from STRÅNG extracted for the Forsmark location was used in the same way, but without the linear regression correction.

The hydrological catchment delineation used in the MIKE SHE modelling (Werner et al. 2013) was further provided by SKB and used as the area of interest when extracting land surface characteristics and parameter values from the ECOCLIMAP-SG database (Masson et al. 2003, CNRM 2018, Druel et al. 2022). The SKB land cover mapping (Löfgren 2010) was further provided by SKB and used for comparison with the data extracted from ECOCLIMAP-SG.

### 2.3.2 Krycklan/Svartberget and Norunda

ICOS Sweden (http://icos-sweden.se) is the Swedish contribution to the Integrated Carbon Observation Systems ICOS (https://www.icos-cp.eu). ICOS is a pan-European network of ecosystem greenhouse gas exchange monitoring sites, where fluxes of carbon between the atmosphere and the land surface as well as related meteorological and ecosystem variables are measured and made publicly available. The measurements include all necessary meteorological variables, such as shortwave, longwave and net radiation, ground heat flux, as well as the sensible and latent heat fluxes, where the latter can be transformed into evaporation. Data from two of the Swedish ICOS sites representing boreal forest landscapes were thus chosen to be included in this study. The Norunda site in northern Uppland (60°05′N, 17°29′E, 46 m a.s.l.; Mölder et al. 2022) is located about 50 km SW of Forsmark, approximately on the same latitude but clearly away from the coastal area. The Svartberget site (64°15′N, 19°46′E, 270 m a.s.l.; Peichl et al. 2022) is located in the region of Västerbotten, at a similar distance from the Swedish east coast as the Norunda site but at slightly higher altitude. Co-located to the Svartberget ICOS station is the Krycklan research catchment (Laudon et al. 2013, from where additional data were provided for the study. ICOS data from Norunda and Svartberget from the period 2014–2016 were retrieved from the ICOS data portal (https://www.icos-cp.eu), whereas Krycklan data was provided by Swedish University of agricultural Sciences (SLU) in Umeå. The data used in this study from these sites are summarized in Table 2-2.

**Table 2-2. Data from the ICOS Norunda and Svartberget sites and the Krycklan research catchment.**

| Variable | Time resolution | Height | Location/comment | Data source |
|---|---|---|---|---|
| *Inputs to the potential evapotransporation calculations* | | | | |
| Air pressure | 30 min | 1.5/2 m | Norunda/Svartberget | ICOS |
| Air temperature | 30 min | 36.8/35 m | Norunda/Svartberget | ICOS |
| Relative humidity | 30 min | 36.8/34.5 m | Norunda/Svartberget | ICOS |
| Wind speed | 30 min | 36.8/34.5 m | Norunda/Svartberget | ICOS |
| Global radiation | 30 min | 55/50 m | Norunda/Svartberget | ICOS |
| Precipitation | daily | 1.5 m/0.3 m and 2.38 m | Norunda/Svartberget | ICOS |
| *Data for calibration and evaluation* | | | | |
| Shortwave radiation up/down | 30 min | 55/50 | Norunda/Svartberget | ICOS |
| Longwave radiation up/down | 30 min | 55/50 | Norunda/Svartberget | ICOS |
| Net radiation | 30 min | 55/50 | Norunda/Svartberget | ICOS |
| Albedo | daily | 55/50 | Derived from shortwave up/down | calculated |
| Latent heat flux | 30 min | 36/34 | Norunda/Svartberget | ICOS |
| Evapotranspiration | daily | 36/34 | Derived from latent heat flux | calculated |
| Cloudiness | hourly | - | Films Kyrkby, Kerstinbo, Uppsala flygplats | SMHI |
| Wind speed | hourly | 10 m | Films Kyrkby, Kerstinbo, Uppsala flygplats | SMHI |
| Snow depth | 30 min | - | Norunda/Svartberget | ICOS |

Continuous time-series of daily values were generated by aggregating the original 30-minute data to daily means (all variables except for precipitation) and sums (precipitation). Albedo was calculated as the ratio of daily mean upwards and downwards shortwave radiation. Daily evapotranspiration (mm $d^{-1}$) was calculated from the daily mean latent heat flux (W $m^{-2}$) by multiplication with 0.0864 Ms $d^{-1}$ and division by the latent heat of vaporisation ~2.5 MJ $kg^{-1}$.

The Norunda main tower sites is surrounded by mature forest stands dominated by Scots pine and Norway spruce with average canopy height 27.5 m. The roughness length for momentum has been estimated to 1.75 m, zero-plane displacement height to 21.1 and leaf area index around 4 (Mölder et al. 2022) which is compared to values extracted from the ECOCLIMAP-SG database (Section 2.3.3). The Svartberget main forest site is surrounded by forest stands dominated by Norway spruce with average canopy height 18 m. Local estimates of roughness length for momentum, zero-plane displacement height and leaf area index were not available for this study, and values extracted from the ECOCLIMAP-SG database was used (Section 2.3.3).

### 2.3.3 ECOCLIMAP global land surface parameter database

ECOCLIMAP (Masson et al. 2003, CNRM 2018) is a global database of land surface parameters developed by Meteo-France and CNRM (Centre National de Recherches Météorologiques) to provide data for initialization of land surface schemes in meteorological and climate models. ECOCLIMAP-SG (Druel et al. 2022) is the second generation of the database, providing data at 300 m resolution world-wide based on the European Space Agency Climate Change Initiative land cover data (ESA 2017).

In ECOCLIMAP-SG, the land surface is represented by 33 surface types (ocean, lakes, rivers, 20 terrestrial nature types, and 10 urban surface types), where the 20 terrestrial nature types includes bare soil and bare rock, permanent snow (glaciers and snow fields), 8 different forest types (boreal broad leaf deciduous, boreal needle leaf deciduous/evergreen, temperate broadleaf deciduous/evergreen, temperate needleleaf evergreen, and tropical broadleaf deciduous/evergreen), shrubs, boreal/temperate/tropical grassland, winter/summer C3 crops, C4 crops, flooded tree cover and flooded shrubs.

For each surface type, parameters needed for calculation of potential evapotranspiration with the Penman-Monteith equation are provided, such as canopy height, leaf area index, vegetation and soil albedo, minimum surface resistance, as well as parameters characterizing the stomata response to global radiation, air temperature and specific humidity of the air. These parameters are compiled from a variety of open data sources, including several satellite based data such as leaf area index and albedo from the EC Copernicus Global Land monitoring service (https://land.copernicus.eu/global) and tree height from the NASA Remote sensing of forests and wetlands service (https://landscape.jpl.nasa.gov). Detailed information about the data sources used to build ECOCLIMAP-SG can be found in the technical documentation provided by CNRM (2018).

Parameters needed for the Penman-Monteith (Monteith 1965) equation are extracted from the ECOCLIMAP-SG database for the Forsmark, Krycklan study areas at 300 m resolution for the extent of the watershed delineations provided by SKB and SLU Umeå, respectively. For the Norunda study area, a buffer area of 5 km around the main tower site was used for the extraction, to provide a reasonable representation of the footprint of the measured turbulent heat fluxes. The fraction of different land cover types and the corresponding parameters within the areas of interests are aggregated by nature cover types within the areas of interest, to enable calculation of potential evapotranspiration for each vegetation type separately, and for spatial aggregation to mean areas over the study areas.

A summary of the data extracted from the ECOCLIMAP-SG database for the 3 study areas is provided in Table 2-3 (areal fractions of land cover types and vegetation cover types in the extracted areas) and Table 2-4 (land surface parameters for evapotranspiration calculations).

**Table 2-3. Fraction of ECOCLIMAP-SG land cover types within the study areas.**

| ECOCLIMAP-SG parameters | Forsmark | Norunda | Svartberget/Krycklan |
|---|---|---|---|
| Area of extracted domain (km$^2$) | 29.1 | 78.5 | 67.8 |
| Latitude (dec. deg.) | 60.38 | 60.08 | 64.25 |
| Longitude (dec. deg.) | 18.20 | 17.45 | 19.80 |
| *Fraction of land cover types* | | | |
| Sea | 1.5 % | 0.0 % | 0.0 % |
| Water | 3.4 % | 2.0 % | 0.1 % |
| Lake | 3.4 % | 2.0 % | 0.1 % |
| River | 0.0 % | 0.0 % | 0.0 % |
| Nature | 91.0 % | 98.0 % | 99.9 % |
| Town | 4.1 % | 0.0 % | 0.0 % |
| *Fraction of vegetation patches in the nature cover type* | | | |
| Bare soil | 0.0 % | 0.0 % | 1.2 % |
| Boreal broadleaf deciduous | 0.0 % | 0.0 % | 0.1 % |
| Temperate broadleaf deciduous | 2.1 % | 4.6 % | 0.0 % |
| Boreal needleleaf evergreen | 74.9 % | 82.3 % | 94.3 % |
| Temperate needleleaf evergreen | 2.5 % | 0.0 % | 0.0 % |
| Shrubs | 2.6 % | 1.0 % | 1.5 % |
| Temperate grassland | 3.0 % | 1.5 % | 1.6 % |
| Winter C3 crops | 4.9 % | 8.3 % | 0.7 % |
| Shrub or herbaceous cover flooded | 1.0 % | 0.0 % | 0.6 % |

All study areas are dominated by the vegetation type Boreal needleleaf evergreen (trees), that cover between 75–95 % of the nature cover, which in turn covers between 91 % and 100 % of the areas. It could be noted that there is no separation between for instance Scots Pine and Norway Spruce in the ECOCLIMAP-SG database, which thus consider these different tree species as similar functional types as represented by the different vegetation types in the database. The fraction of lakes and flooded land is about 4 % in Forsmark catchment areas, 2 % in the area extracted for Norunda, and only about 0.1 % within the Krycklan catchment.

The distribution of land cover and vegetation types within the Forsmark area have also been compared to the more detailed data provided by Löfgren (2010). The largest discrepancy is found for the lake and wetland areas, which cover about 8 % and 10 % of the Forsmark area, respectively, according to Löfgren (2010). Possibly, this is due to a mismatch in the classification of shrubs, temperate grassland and shrub or herbaceous cover flooded in ECOCLIMAP-SG versus wetland and mires as classified in Löfgren (2010). There is also a large discrepancy in the fraction of built-up areas and sea, which suggests that the areas considered in the analyses might not be exactly the same.

The ECOCLIMAP-SG land surface parameters extracted for the Penman-Monteith equation (Table 2-4) can be further compared with local estimates and parameters used by FAO (Allen et al. 1998) and Eriksson (1981). For instance, tree height seems to be almost correct in Forsmark and Svartberget – around 15 m and 17 m, respectively – but somewhat underestimated for Norunda (around 18 m compared to 27.5 m from local estimates). Leaf area index of the dominating tree type (boreal needleleaf evergreen) is close to 4 $m^2\ m^{-2}$ for Forsmark and Norunda, which is close to local estimates, and a bit lower for the Svartberget area (3 $m^2\ m^{-2}$) as expected. Albedo values from ECOCLIMAP-SG are somewhat lower than the values used for the FAO reference evapotranspiration (0.23) and by Eriksson (1981) who used albedo = 0.12 for snow free-conditions. Comparison with albedo estimated from the upwards and downwards shortwave radiation measurements in Norunda and Svartberget is included in the results section. Parameter definitions and usage in the Penman and Penman-Monteith equations are further discussed in Section 2.2 above.

**Table 2-4. Land surface parameters extracted from the ECOCLIMAP-SG database for Forsmark, Norunda and Svartberget/Krycklan study areas, used as input to the Penman-Monteith potential evapotranspiration equation.**

| Land cover type / study area | $z_c$ | $z_{0m}$ | d | LAI** | Albedo | $r_{s,min}$ | $r_{gl}$ | $\gamma$ |
|---|---|---|---|---|---|---|---|---|
| *Forsmark* | | | | | | | | |
| Temperate broadleaf deciduous | 14.8 | 1.930 | 9.9 | 4.25 | 0.091 | 150 | 30 | 0.04 |
| Boreal needleleaf evergreen | 15.7 | 2.040 | 10.5 | 3.94 | 0.087 | 150 | 30 | 0.04 |
| Temperate needleleaf evergreen | 5.0 | 0.650 | 3.4 | 2.37 | 0.087 | 150 | 30 | 0.04 |
| Shrubs | 16.1 | 2.088 | 10.8 | 4.88 | 0.090 | 150 | 30 | 0.04 |
| Temperate grassland | 0.9* | 0.106 | 0.6 | 4.88 | 0.088 | 40 | 100 | 0 |
| Winter C3 crops | 1.0* | 0.125 | 0.7 | 4.28 | 0.090 | 40 | 100 | 0 |
| Shrub or herbaceous cover flooded | 0.4* | 0.047 | 0.3 | 2.18 | 0.086 | 40 | 100 | 0 |
| *Norunda* | | | | | | | | |
| Temperate broadleaf deciduous | 17.6 | 2.285 | 11.8 | 4.65 | 0.102 | 150 | 30 | 0.04 |
| Boreal needleleaf evergreen | 18.2 | 2.371 | 12.2 | 3.93 | 0.090 | 150 | 30 | 0.04 |
| Shrubs | 17.5 | 2.279 | 11.7 | 4.62 | 0.109 | 150 | 30 | 0.04 |
| Temperate grassland | 0.8 | 0.099 | 0.5 | 4.59 | 0.107 | 40 | 100 | 0 |
| Winter C3 crops | 0.9 | 0.113 | 0.6 | 3.99 | 0.114 | 40 | 100 | 0 |
| Summer C3 crops | 0.8 | 0.100 | 0.5 | 3.92 | 0.113 | 40 | 100 | 0 |
| *Svartberget/Krycklan* | | | | | | | | |
| Bare soil | 0 | 0.013 | 0 | 0 | 0.085 | n.a. | n.a. | n.a. |
| Boreal broadleaf deciduous | 17.0 | 2.210 | 11.4 | 4.50 | 0.084 | 150 | 30 | 0.04 |
| Boreal needleleaf evergreen | 17.8 | 2.312 | 11.9 | 3.00 | 0.085 | 150 | 30 | 0.04 |
| Shrubs | 16.0 | 2.085 | 10.7 | 3.16 | 0.086 | 150 | 30 | 0.04 |
| Temperate grassland | 0.5 | 0.065 | 0.4 | 2.98 | 0.086 | 40 | 100 | 0 |
| Winter C3 crops | 1.0 | 0.120 | 0.7 | 3.83 | 0.092 | 40 | 100 | 0 |
| Shrub or herbaceous cover flooded | 0.5 | 0.058 | 0.3 | 2.67 | 0.085 | 40 | 100 | 0 |

* Heights of low vegetation types were inferred from the roughness length using $z_{0m} = 0.123 \times z_c$.

** Most of the vegetation types have seasonal variation in leaf area index, and values here are for 1 July.

# 3 Results and discussion

## 3.1 Available energy for evapotranspiration

In this section, the impact of the identified deviations in the following three methods to estimate the available energy for evapotranspiration are compared: i) the methods used by SMHI to generate the input to the Penman (1948, 1956) equation following Eriksson (1981), ii) the methods suggested by Allen et al. (1998) used for inputs to the FAO reference evapotranspiration, and iii) the revised methods used for input to the application of the Penman-Monteith (Monteith 1965) equation introduced in this report.

The overall workflow is identical in all three methods, following the steps outlined in Section 2.2.2. Important deviations were identified in the steps dealing with cloudiness and atmospheric turbidity, net longwave radiation, as well as the albedo and the resulting net shortwave radiation. The impact of these features on the resulting net radiation and its components is presented in the following.

Each section starts with a short reminder about the role of the variable assessed in the section, and a summary of the models presented in the results. After each result sub-section, a short concluding remark and recommendation are also provided.

### 3.1.1 Cloudiness and atmospheric turbidity

The turbidity (τ) is used to infer cloudiness ($C$) from global radiation ($R_s$) using Equation A-13, and to estimate the clear-sky radiation from the extra-terrestrial radiation ($R_{so} = \tau_{max} R_{ext}$). $C$ is further used to estimate net longwave radiation ($R_{nl}$) with Equation 2-17 following Eriksson (1981), propagating into the inputs for Penman-SMHI. For the revised calculations of PET using Penman and Penman-Monteith following this report, $R_{so}$ is used to calculate relative sunshine ($R_s/R_{so}$) which is used in Equation 2-17 following Allen et al. (1998), which propagates into the estimation of net radiation and eventually PET. The models compared in this section are:

- **Constant (FAO-98),** using constant minimum and maximum τ-values throughout the year.
- **Sun angle (FAO-98)**, where $\tau_{max}$ and $\tau_{min}$ are functions of solar angle (Equation A-14).
- **Seasonal (Eriksson-81),** using one set of $\tau_{max}$ and $\tau_{min}$ values for summer and one for winter.

As identified in Section 2.2.2, the FAO used a constant minimum (0.25) and maximum (0.75) turbidity representing 100 % overcast and clear-sky conditions, respectively, whereas Eriksson (1981) used different values for the summer (0.22; 0.81) and winter (0.15; 0.77) seasons. In both cases, the cloudiness is assumed to change linearly between 0 and 1 as the turbidity change between its minimum and maximum values. FAO further recommend that for high latitude areas, it might be important to consider the lowering impact of low solar angles on the turbidity. Thus, they provide equations for estimation of the turbidity as a function of latitude and day of the year.

In Figure 3-1, the different turbidity models are compared with the turbidity derived from the observed global radiation at the three study areas. The range between minimum and maximum observed turbidity show a clear seasonal pattern at all three sites, in line with the predictions by the Eriksson (1981) and the solar angle model from FAO. Both minimum and maximum values are lower in winter than in summer, as predicted by these two models in various degree (Figure 3-1), However, there is a clear difference in the results based on the global radiation data from Forsmark compared to the other two sites. The Forsmark data is almost perfectly encompassed by the solar-angle predictions of minimum and maximum turbidity during 2014–2015, whereas the data from 2016–2017 and from Norunda and Svartberget during the entire period show a larger range of turbidity values also in winter, more in line with the simplified seasonal model of Eriksson (1981) (Figure 3-1). The reason for this different behaviour could represent real differences in the atmospheric conditions at the site, but it could also be due to local disturbances, sensor height above the ground or changes in the measurement equipment. The fact that behaviour of the Forsmark global radiation and turbidity data is changing over time makes the latter explanation plausible, but it should be confirmed with information on the sensor and installation history.

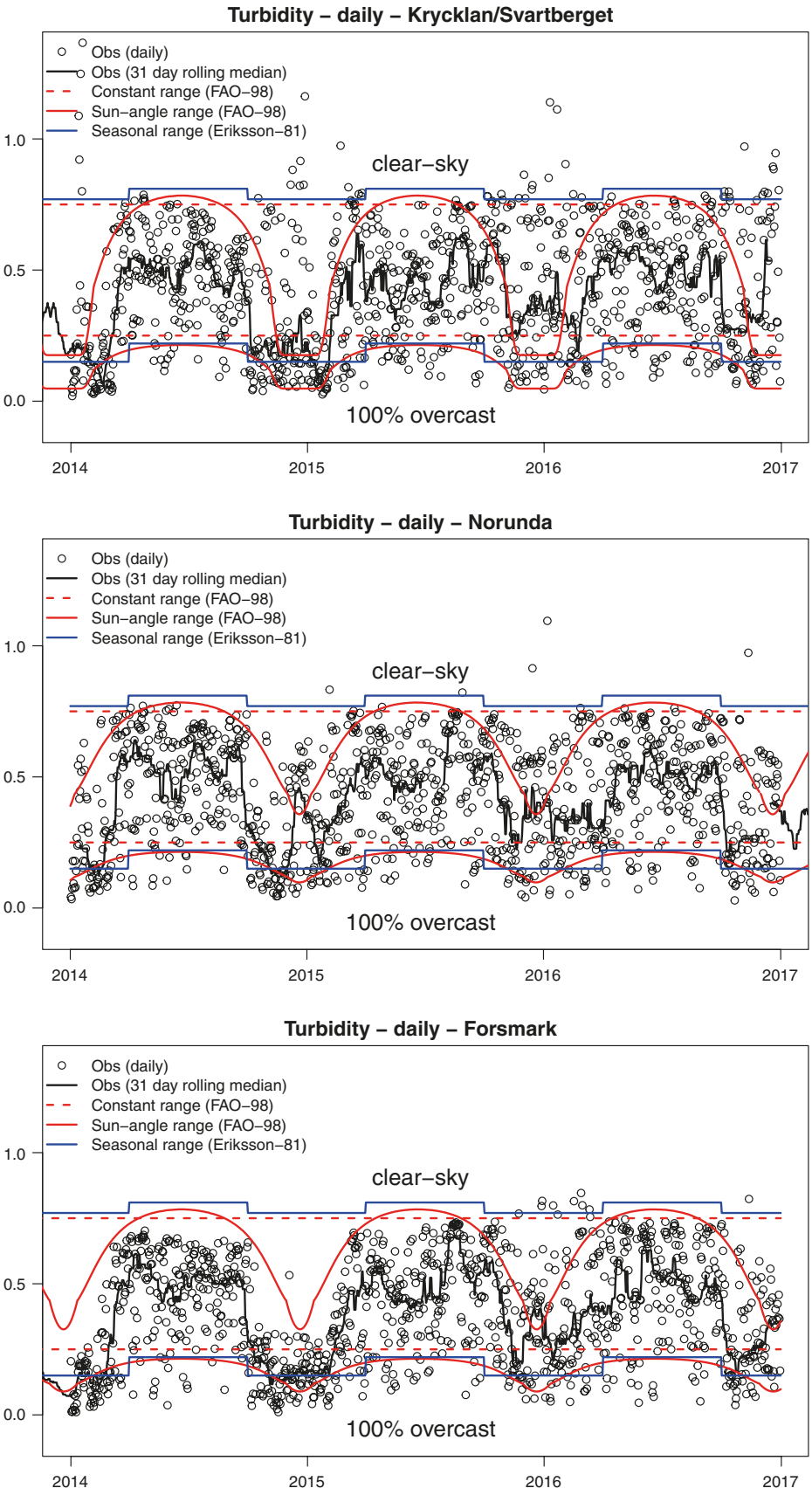


***Figure 3-1.*** *Minimum and maximum atmospheric turbidity (ratio between global radiation and extra-terrestrial radiation at 100 % overcast and clear-sky conditions, respectively) at the 3 study sites, (top) Krycklan/Svartberget, (middle) Norunda, and (bottom) Forsmark estimated by the FAO-98 constant range (red dashed lines), the Eriksson-1981 separate ranges for summer and winter (blue solid lines), the FAO-98 sun-angle dependency recommended for latitudes > 50 °N (red solid lines), and by the observed global radiation (black markers and solid lines).*

The solar angle method improves the results of estimating cloudiness for the Forsmark area when comparing to the cloudiness observation from the SMHI stations at Örskär and Films (Table 3-1). At Norunda and Svartberget, the simplified seasonal turbidity-based cloudiness estimation used by Eriksson (1981) was superior to the other methods.

Based on these results, the Eriksson (1981) turbidity model was concluded to be most robust of the three investigate models, and was used for the remaining calculations steps assessed in this report.

**Table 3-1. Cloudiness modelling at Forsmark and Norunda evaluation using observations from assessment at surrounding SMHI stations; KGE = Kling Gupta model efficiency index*, RE = relative error (%).**

| Stations | | | Turbidity models | | | | | |
|---|---|---|---|---|---|---|---|---|
| Radiation | Cloudiness | Period | Constant | Seasonal | Sun-angle | Constant | Seasonal | Sun-angle |
| | | | KGE* | KGE* | KGE* | RE | RE | RE |
| Forsmark | Örskar | 2014-16 | 0.61 | 0.62 | **0.76** | 33 % | 30 % | **11 %** |
| | Films | 2005-08 | 0.63 | 0.64 | **0.76** | 23 % | 20 % | **5 %** |
| | Films | 2014-16 | 0.75 | 0.75 | **0.78** | 12 % | 10 % | **−5 %** |
| Norunda | Films | 2014-16 | **0.82** | **0.82** | 0.72 | 4 % | **1 %** | −14 % |
| | Kerstinbo | 2014-16 | 0.79 | 0.80 | 0.74 | 7 % | **5 %** | −11 % |
| | Uppsala | 2014-16 | 0.77 | 0.80 | 0.75 | 14 % | 12 % | **−6 %** |

* Kling-Gupta efficiency (Gupta et al. 2009) measures the ability of a model to predict an observation that combines correlation between the two time-series with relative errors in the mean and standard deviation. KGE varies between −1 (very low performance) to 1 (perfect model).

### 3.1.2 Net longwave radiation

Net longwave radiation (upwards) is calculated with Equation 2-17 and propagates into estimation of net radiation ($R_n$) (Equation 2-18), Ground heat flux (Equation 2-10) and eventually PET (Equations 2-6, 2-8, 2-10, 2-11). The models compared in Figure 3-2 are:

- **FAO-56**, Equation 2-17 following FAO, using $R_s/R_{so}$ based on the Eriksson (1981) turbidity model,
- **B. Eriksson**, Equation 2-17 following Eriksson (1981), using $C$ based on the Eriksson (1981) turbidity model, and further propagating into the inputs to Penman-SMHI, and
- **Brunt, calibrated**, Equation 2-17 with calibrated coefficients, also $R_s/R_{so}$ based on the Eriksson (1981) turbidity model.

Observations of net radiation and its components (upward and downward shortwave and longwave radiation) and ground heat flux were only available from the Norunda and Krycklan/Svartberget study areas. The Forsmark area is thus omitted from the assessment of these variables in the following Sections 3.1.2 to 3.1.5.

The magnitude of the observed net longwave radiation varies between about 1–6 MJ $m^{-2}$ $day^{-1}$ for the study areas. This is small compared to the magnitude of the net shortwave radiation that varies between 0–20 MJ $m^{-2}$ $d^{-1}$. However, downward and upward longwave radiation have a similar seasonal variation (not shown), which explains why the net longwave radiation shows a much smaller seasonal variation than the net shortwave. Net longwave is larger than the net shortwave radiation only during the period from November to March (Figure 3-2 versus Figure 3-4 and Figure 3-5) It should also be noted that the results presented in Figure 3-2 are weekly mean values, aggregated over several years (2014–2016), and that the net longwave radiation may be larger for individual days.

The choice of equation for the net longwave radiation generated a difference of almost 50 % between the highest (Eriksson, 1981) and the lowest (FAO) estimates. As noted in Section 2.2.2, both of these methods are using the same equation from Brunt (1932), but with different parameter values, and slightly different definition of the input variables. The calibrated Brunt equation, using the inputs as defined by FAO and calibrated using the longwave data from Norunda and Svartberget/Krycklan showed results very close to the observations (Figure 3-2). Please note that the parameters were calibrated combining data from both sites to avoid overfitting to either of them In addition only a sub-set of the data was used for calibration. The values of the calibrated Brunt parameters were $b_1 = 0.294$, $b_2 = 0.066$, $b_3 = -0.055$, and $b_4 = 1.055$.

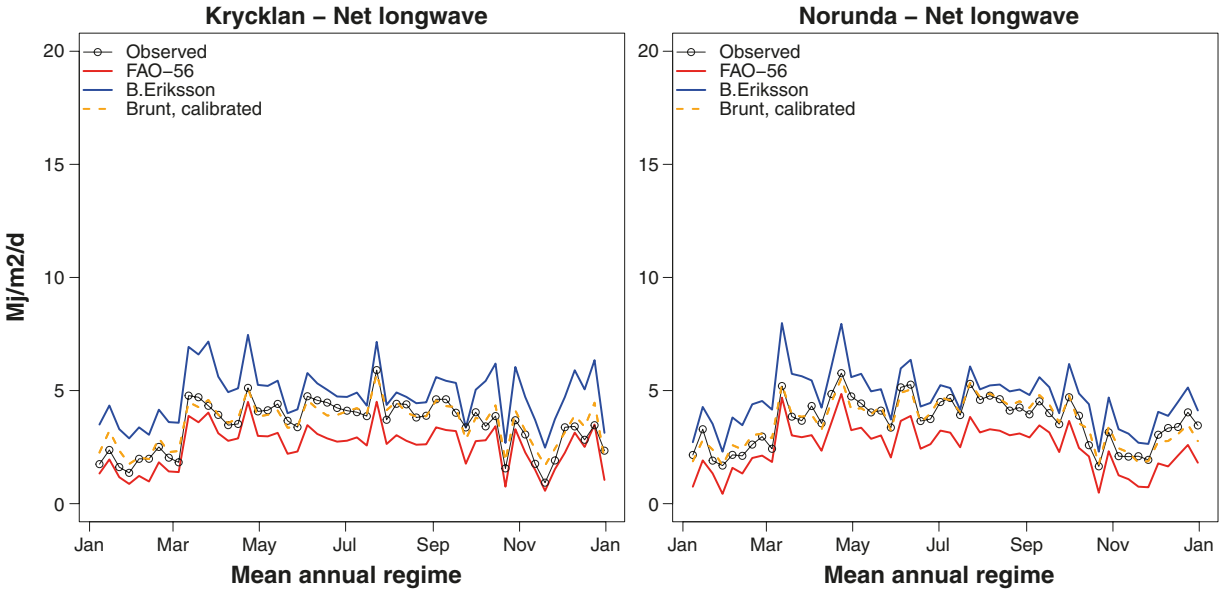


***Figure 3-2.*** *Net longwave radiation (upward–downward) estimated for the Krycklan/Svartberget (left) and Norunda (right) sites following Eriksson (1981; blue line), FAO (1998; red line) and the revised method (orange dashed line) combining atmospheric turbidity model by Eriksson (1981) and net longwave formula from Brunt (1932) with parameters calibrated using the Norunda and Svartberget ICOS data (black line and symbols). The annual regimes are based on time-series of daily data for the period 2014–2016 aggregated to a weekly time resolution.*

Based on these results, the Brunt (1932) equation, as defined by FAO (Equation 2-17), with the parameters calibrated with Norunda and Svartberget/Krycklan data is recommended for further use, and adopted for the remainder of this report.

### 3.1.3 Albedo and net shortwave radiation

Albedo is a key variable for estimating the net shortwave radiation using Equation 2-16, and is propagating into the estimation net radiation, ground heat flux and PET. Three albedo models are compared in Figure 3-3 and their impact on net shortwave radiation in Figure 3-4. These models are:

- **FAO**, constant albedo value of 0.23 following FAO (Allen et al. 1998).
- **B. Eriksson**, 0.12 without snow and 0.5 with snow on the ground (Eriksson 1981).
- **Dual source**, effective albedo considering the transmission of radiation between a vegetation layer and the ground below (Equation 2-15), with leaf area index, soil and vegetation albedo from ECOCLIMAP-SG for the case study areas, and snow albedo simulated with a simple snow model (Appendix A, Section A3).

Similar to the analysis of net longwave radiation, results for the Forsmark area is omitted in this assessment due to the lack of observations, see Section 3.1.2.

The FAO reference evapotranspiration method uses a constant albedo value of 0.23, whereas the previous SMHI method uses 0.12 for snow-free conditions and 0.50 when there is snow on the ground (Eriksson 1981). In the dual-source evapotranspiration model, the vegetation and ground layer albedo values varies between about 0.08 and 0.12 for snow free conditions (Table 2-4), and account for values up to 0.9 when the ground is covered by fresh snow or when the canopy height is lower than the snow depth (snow model description is provided in Appendix A, Section A3). In addition to the albedo of the different vegetation types and the different snow types, the leaf area index, which varies within the year and between vegetation types, and the fractional area of the different vegetation types affects the final mean effective albedo.

Comparison of simulated and observed albedo showed that for the type of boreal forests represented by the study areas, the constant albedo of 0.23 recommended for the FAO reference evapotranspiration largely overestimate albedo in summer and underestimate the albedo in winter (Figure 3-3). The results further show that the drastic switch of albedo from 0.12 in snow free conditions to 0.5 with snow on the ground, as suggested by Eriksson (1981) also does not fit the boreal forests conditions during winter. The dual-source model, simulated effective land surface albedo very close to the observations during summer, and somewhat closer to the observations in winter than the other models (Figure 3-3). As noted, this model was developed using the values for leaf area index, albedo and canopy height for the different land surface types in the study areas, as represented in the ECOCLIMAP-SG database, plus the simulate snow cover and snow surface albedo. It means that it is considerably more complex than the simplified methods suggested by FAO and Eriksson (1981). Still, the impact of intercepted snow on the forest canopies was also not considered in these calculations with the dual-source model, which could be one explanation for the deviating results compared with observations during winter.

To conclude, as the albedo calculations are greatly improved by the dual-source model as compared to Eriksson (1981) and FAO, this methodology is recommended for further use. The impacts on $R_n$ and PET of using the FAO and Eriksson (1981) albedo models are further examined in the Section 3.1.4 and 3.2.

The errors in the calculated albedo propagates into the calculation of net shortwave radiation. Specifically, a certain error in albedo during summer, when global radiation is high, will have a larger impact on the net radiation than a corresponding error during winter. Consequently, the overestimation of summer-time albedo by the FAO constant albedo model (Figure 3-3) generates a large underestimation of net shortwave radiation in summer, whereas a relatively small differences in the winter-time net shortwave despite is generated by the relatively large error in albedo used by Eriksson (1981). Due to the snow-free albedo of 0.12, the Eriksson (1981) model results in rather small underestimation of net shortwave radiation in summer, whereas the overestimated albedo for snow covered ground in the model has a clear negative impact on net shortwave radiation in the winter/spring season. This pattern is especially apparent at the Svartberget/Krycklan site where the snow cover remains longer into the year. The errors in net shortwave radiation are smaller with the dual-source model than with the Eriksson and FAO models, although a slight underestimation can be seen during the transition from winter to spring in the Svartberget/Krycklan results (Figure 3-4) corresponding to the overestimation of albedo in the same period (Figure 3-3).

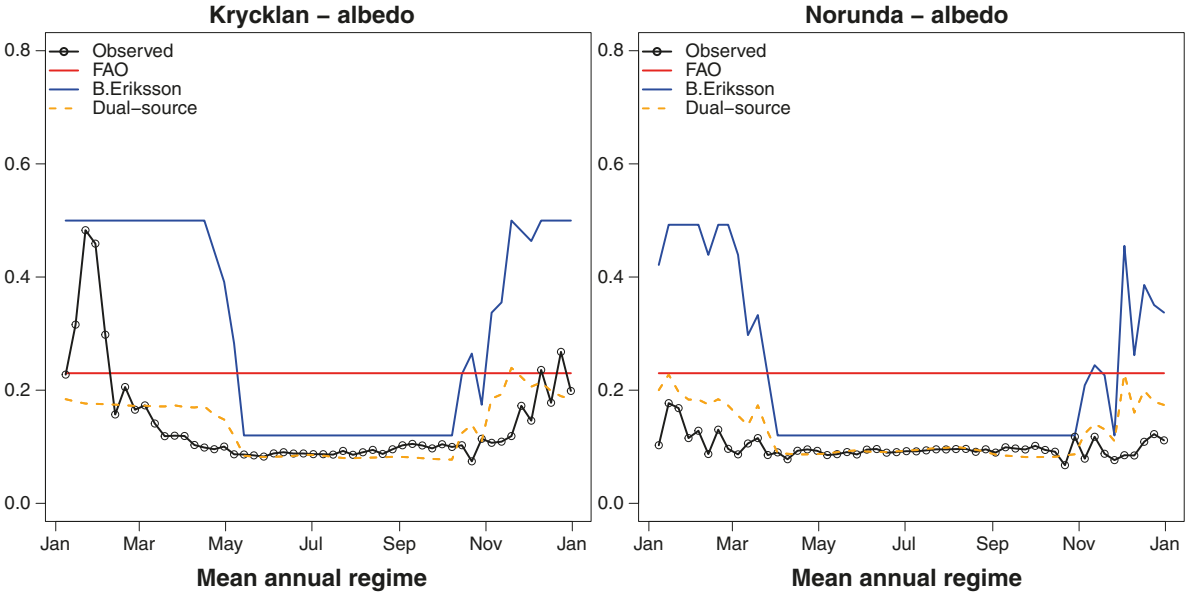


***Figure 3-3.*** *Albedo (fraction of downward shortwave radiation reflected by the land surface) estimated for the Krycklan/Svartberget (left) and Norunda (right) sites following FAO (1998; red line), Eriksson (1981; blue line), and the dual-source radiation transmission model (orange dashed line) combining leaf area index, albedo of vegetation and soil extracted from the ECOCLIMAP database for the respective areas, and snow-age dependent snow albedo, compared to albedo derived from the shortwave radiation observations (black lines and symbols). The annual regimes are based on time-series of daily data for the period 2014–2016 aggregated to a weekly time resolution.*

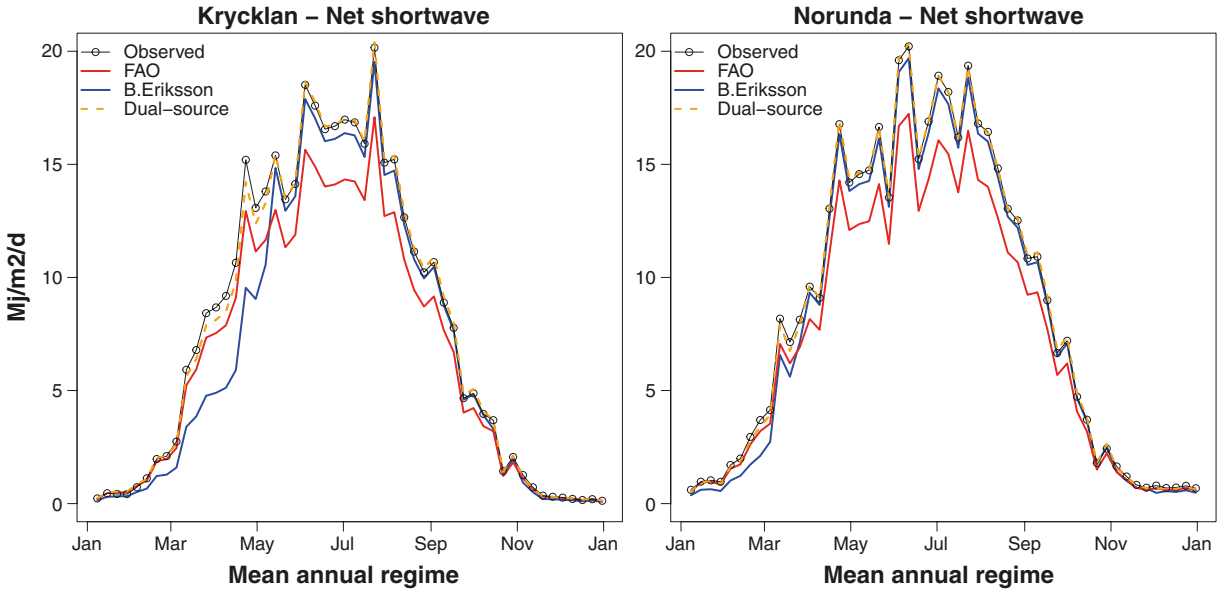


***Figure 3-4.*** *Net shortwave radiation estimated for the Krycklan/Svartberget (left) and Norunda (right) sites following FAO (1998; red line), Eriksson (1981; orange dashed line), and the dual-source radiation transmission model (orange dashed line) as parameterised in this study, compared to the observations from the ICOS stations (black lines and symbols). The annual regimes are based on time-series of daily data for the period 2014–2016 aggregated to a weekly time resolution.*

The results for net shortwave radiation reinforce the previous conclusion that the dual-source model for the effective albedo with vegetation and soil albedo parameters from ECOCLIMAP-SG and simulated snow albedo was the best model of the three tested here.

### 3.1.4 Net radiation

Net radiation is a direct input to the Penman, Penman-Monteith and Priestley-Taylor PET equations, and is calculated with Equation 2-14 and is dependent on the estimation of several input variables that are assessed in Section 3.1.1 to 3.1.3. Three different methods to estimate net radiation are assessed in this section. The model and their names used in Figure 3.1.5 are summarised here:

- **FAO**, based on albedo and net longwave according to FAO (Allen et al. 1998).
- **B. Eriksson**, based on albedo and net longwave according to Eriksson (1981).
- **Dual source, cal.**, based on the dual source albedo (Equation 2-16, Section 3.1.3) and net longwave using Brunt (1932) with parameters calibrated to Norunda and Svartberget data (Section 3.1.2).

The discrepancies in net shortwave and net longwave radiation estimates by the different methods naturally also result in corresponding discrepancies in the net radiation (Figure 3-5). The overestimated albedo by the Eriksson (1981) method leads to a clear underestimation of net radiation during the snow-covered part of the year, which was a larger problem at the Svartberget/Krycklan site than at the Norunda site when compared to the observed net radiation. The use of a constant albedo of 0.23 following the FAO recommendation was identified to be a greater problem during summer than during winter (Section 3.1.3), since the boreal forests in the study areas had an albedo closer to 0.10 according to the upward/downward shortwave radiation measurements. Thus, following the FAO recommendation, the net radiation is underestimated in summer and slightly overestimated in winter. Net radiation estimated with the dual-source model – including distribution of radiation between the canopy and ground layers, and the locally calibrated Brunt equation for longwave radiation – on the other hand performed very well compared to the observations both in winter and summer (Figure 3-5).

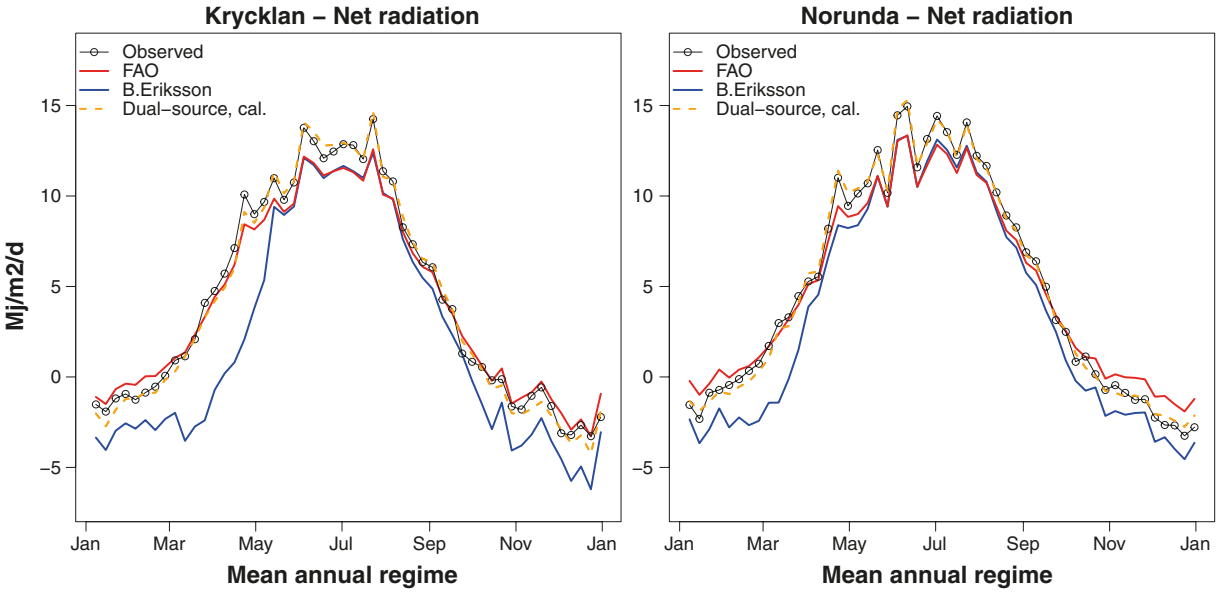


***Figure 3-5.*** *Net radiation at the Svartberget/Krycklan and Norunda study sites, observations (black lines and symbols) compared to calculations with albedo and net longwave radiation formulations according to FAO (Allen et al. 1998) (red line), Eriksson (1981) (blue line), and the dual-source model with leaf-area-index and albedo of vegetation and ground according to ECOCLIMAP-SG, and the locally calibrated version of the Brunt formula (orange dashed line). The annual regimes are based on time-series of daily data for the period 2014–2016 aggregated to a weekly time resolution.*

The assessment of the net radiation estimates using statistical model performance indicators (Table 3-2) further demonstrates that the main problem in the Eriksson (1981) method as implemented by SMHI for the calculation of Penman-SMHI is the overestimated net longwave radiation, leading to an underestimation of net radiation of 30 % and 54 % at the two sites. The analysis also shows that the underestimation of both net (downward) shortwave and net (upward) longwave radiation using the FAO method evened out to an average error in net radiation of less than 5 % (Table 3-2). The combination of the dual source radiation transmission model for the net shortwave radiation and the calibrated Brunt equation for the net longwave radiation showed overall small errors, less than 5 %, for all radiation components during all seasons of the year (Table 3-2 and Figure 3-5).

As a conclusion, for estimation of net radiation as input to PET calculations, it is recommended to i) use the Brunt (1932) equation for net longwave radiation following FAO with parameters adjusted to local conditions if possible, and ii) use a dual source radiation transmission model for estimating the effective albedo over vegetated areas, with adequate parameters for the albedo of vegetation, soil and snow. Net radiation estimated according to Eriksson (1981) will be further used to assess its importance for the Penman-SMHI PET estimates.

**Table 3-2. Evaluation of net radiation estimates for the Norunda and Svartberget/Krycklan ICOS sites following the methods of FAO (Allen et al. 1998), BE (Eriksson 1981) and the dual source (DS) method combined with re-calibrated Brunt equation described in this report. The model performance indicators are mean values of observed (Mobs) and estimated data (Msim), the relative error in the estimates (RE) and the Kling-Gupta model efficiency index (KGE*) based on daily data.**

| Station | Variable | Model | Mobs | Msim | RE | KGE* |
|---|---|---|---|---|---|---|
| Norunda | Albedo | FAO | 0.10 | 0.23 | 132 % | n.a. |
| | | BE | | 0.22 | 121 % | −2.17 |
| | | DS | | 0.12 | 23 % | 0.24 |
| | $R_{sn}$ | FAO | 8.58 | 7.32 | −15 % | 0.79 |
| | | BE | | 8.12 | −5 % | 0.95 |
| | | DS | | 8.57 | 0 % | 0.99 |
| | $R_{ln}$ | FAO | 3.64 | 2.50 | −31 % | 0.67 |
| | | BE | | 4.69 | 29 % | 0.47 |
| | | Brunt** | | 3.71 | 2 % | 0.90 |
| | $R_n$ | FAO/FAO | 4.94 | 4.82 | −2 % | 0.83 |
| | | BE/BE | | 3.43 | −30 % | 0.69 |
| | | DS/Brunt** | | 4.86 | −2 % | 0.98 |
| Krycklan | Albedo | FAO | 0.14 | 0.23 | 64 % | n.a. |
| | | BE | | 0.31 | 119 % | −0.41 |
| | | DS | | 0.13 | −4 % | 0.12 |
| | $R_{sn}$ | FAO | 7.67 | 6.55 | −15 % | 0.79 |
| | | BE | | 6.73 | −12 % | 0.87 |
| | | DS | | 7.62 | −1 % | 0.99 |
| | $R_{ln}$ | FAO | 3.45 | 2.54 | −26 % | 0.70 |
| | | BE | | 4.79 | 39 % | 0.40 |
| | | Brunt** | | 3.39 | −2 % | 0.80 |
| | $R_n$ | FAO/FAO | 4.22 | 4.01 | −5 % | 0.85 |
| | | BE/BE | | 1.94 | −54 % | 0.45 |
| | | DS/Brunt** | | 4.23 | 0 % | 0.96 |

* Kling-Gupta efficiency (Gupta et al. 2009) measures the ability of a model to predict an observation that combines correlation between the two time-series with relative errors in the mean and standard deviation. KGE varies between −1 (very low performance) to 1 (perfect model).

** Brunt (1932) net longwave radiation with parameters calibrated using a sub-set of combined data from the Norunda and Svartberget ICOS stations.

### 3.1.5 Ground heat flux

Ground heat flux is a direct input to the Penman, Penman-Monteith and Priestley-Taylor PET equations, and is calculated with Equation 2-20 with net radiation as the only input variable. The sensitivity of the original Gardelin and Lindström (1997) to the different net radiation estimates evaluated in Section 3.1.4, as well as the impact of the modification introduced in Equation 2-20 is assessed in this section. The models tested and their names as presented in Figure 3-6 are:

- **Gardelin-97, old $R_{net}$,** original Gardelin and Lindström (1997) model with net radiation following Eriksson (1981), which is equivalent to the input to Penman-SMHI.
- **Gardelin-97, new $R_{net}$,** original Gardelin and Lindström (1997) model with net radiation following the revised estimate based on the dual-source model from this study.
- **Calibrated, new $R_{net}$,** Equation 2-20 with parameters calibrated to the Norunda and Svartberget/Krycklan data and the dual-source based net radiation as input.

The original Gardelin and Lindström (1997) equation largely overestimates the annual amplitude of the ground heat flux compared to the observations from Krycklan/Svartberget and Norunda (Figure 3-6). The overestimation is apparent for both the improved method to calculate net radiation introduced here (Section 3.1.4) and the estimates following Eriksson (1981). It is interesting to note that the general underestimation of net radiation by the Eriksson (1981) procedure (Figure 3-5, Table 3-1) is here transformed to a ground heat flux that is negative on average using the original Gardelin and

Lindström (1997) parameters, whereas using a more realistic net radiation leads to an average ground heat flux closer to zero, which is to be expected unless the climate is in a cooling period. However, the deviations caused by net radiation did not improve on the magnitude of the seasonal variation of the ground heat flux using the original Gardelin and Lindström (1997) equation, compared to the soil heat flux observation from Norunda and Svartberget. Calibration of the modified function, including positive and negative scaling parameters (Section 2.2.3) was able to fit the data much better, with parameter values $g_{pos}$ = 0.30 and $g_{neg}$ = 0.35 for Svartberget/Krycklan and $g_{pos}$ = 0.15 and $g_{neg}$ = 0.25 for Norunda. The results in Figure 3-6 indicate an increase of the available energy for evaporation ($R_n$-$G$) of around 1.5 MJ m$^2$ d$^{-1}$ in summertime and a decrease of around 1 MJ m$^2$ d$^{-1}$, in addition to the corrected underestimations of net radiation presented in Figure 3-5.

Based on these results it is suggested that the modified Gardelin and Lindström (1997) Equation 2-20 and the calibrated parameters can be used for estimating $G$ from $R_n$, at least for sites similar to Norunda and Svartberget/Krycklan. However, it should be noted that no data representing non-forested conditions was used in the calibration. An alternative approach that was not tested in this study, would be to first distribute $R_n$ between the canopy ($R_{n,canopy}$) and the ground ($R_{n,ground}$) using Equation 2-19, and then derive $G$ with $R_{n,ground}$ as input to Equation 2-20. With this approach, the variation in the exposure of the ground to the radiation caused by the vegetation density would be propagated to the estimation of G, which sounds reasonable from a physical perspective. Given that $R_{n,ground} < R_n$ it is likely that the original Gardelin and Lindström (1997) would provide better results compared to the observations, and that the correction parameters could be set closer to 1 or neglected.

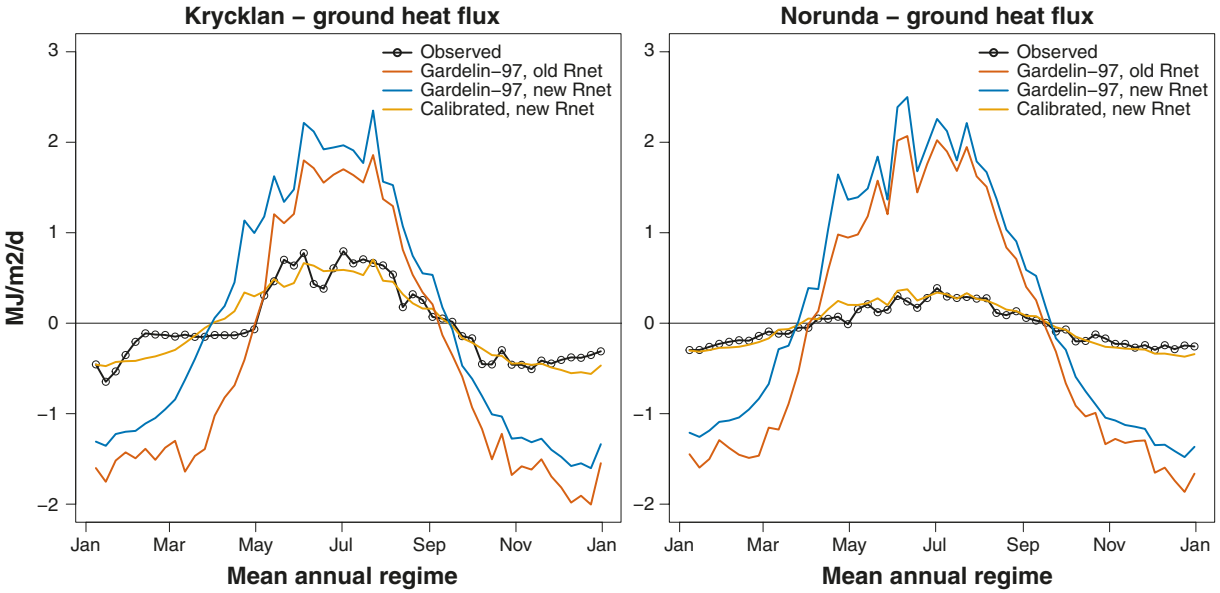


***Figure 3-6.*** *Soil heat flux estimated with the original (red and blue lines) and calibrated (orange line) Gardelin and Lindström (1997) equations using net radiation estimates following Eriksson (1981) (red line) and with the improved net radiation from this study (blue and orange lines) compared with the observed soil heat flux (black circles and line) at the (left) Krycklan/Svartberget and (right) Norunda ICOS stations. Time-series of daily data for the period 2014–2016 were aggregated to a mean annual regime at a weekly time resolution.*

### 3.1.6 Wind speed above forests and open land

The wind speed measured at the Norunda ICOS station at 36 m height is on average 32 %, 10 % and 26 % higher than the wind speed measured at the SMHI weather stations Films, Kerstinbo and Sala, respectively, and 30 % lower than the wind speed measured at Uppsala airport (Figure 3-7).

Using the zero-plane displacement height (21.1 m) and roughness length (1.75 m) estimated by Mölder et al. (1999), the estimated ratio between the forest windspeed at 36 m height and the 10 m wind speed at an open field weather station is 48 % according to Silversides (1978) and 123 % according to the assumption made in Section 2.2.4 of a similar windspeed at 10 m above the zero-plane displacement heights of the open field and the forest.

The relation between the Norunda windspeed and the windspeed measured at the Uppsala airport is thus perfectly in-line with the Silversides (1978) airport to forests predictions, whereas the relation to the other SMHI stations is more in-line with the assumption of a similar windspeed at 10 m above the zero-plane displacement heights (Section 2.2.4). It can also be noted from the lower whiskers (brackets) of the boxplots in Figure 3-7, that the minimum daily mean windspeed in the Norunda dataset is well above 0 m/s (around 0.8 m/s), whereas the minimum daily windspeed reported at all the SMHI stations were close to 0 m/s. The nearest SMHI station to Norunda is the Films station, located roughly mid-way between Norunda and the coastal location of the Forsmark area. This is the station with the highest ratio between mean wind speed above the Norunda forest and the 10 m wind speed at the open field weather station, and the station with the most similar variance in the wind speed to Norunda.

Based on these results, the choice of method for correcting wind speed from measurements at 10 m height above an open area to a representative height above a forest depend on the characteristics of the measurements site. If the measurement station is located in a large exposed flat area, such as an air field or close to the coast, the Silversides (1978) method is probably the best. If it is located in a smaller opening, surrounded by forest areas, the method suggested in Section 2.2.4 might be better. For the Forsmark case, the method suggested in Section 2.2.4 is used for the remainder of the report, assuming that the wind speed station was located relatively close to the forested areas. However, given the proximity to the sea, it would be interesting to further investigate the properties of the wind speed measurements at the Forsmark and Örskär stations in relation to the stations included in the assessment presented in Figure 3-7.

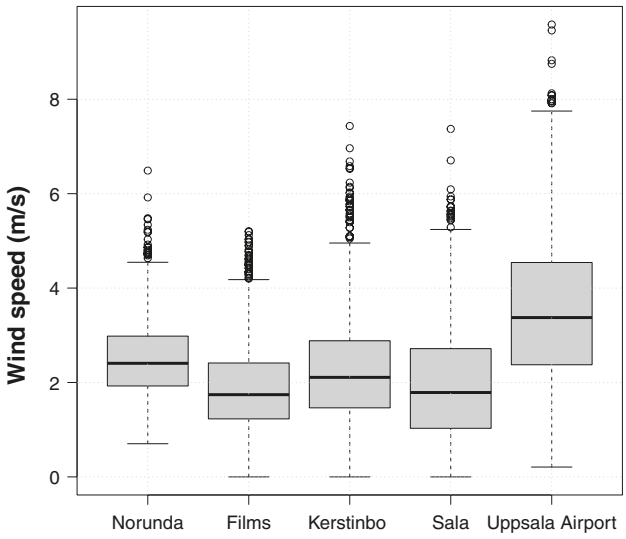


***Figure 3-7.*** *Boxplots of daily mean wind speed measured at the Norunda ICOS station 2014–2016 at 36 m height and at the surrounding SMHI weather stations Films, Kerstinbo, Sala, and Uppsala Airport at 10 m height. The boxes represent the interquartile range, and the horizontal line in the box represent the median of the data. The so-called whiskers represent the minimum and maximum of the data within 1.5 times of the interquartile range. Values outside the whiskers are shown as separate markers.*

## 3.2 Potential evapotranspiration

### 3.2.1 Impact of net radiation, ground heat flux and choice of PET-equation

The impact of the differences in available energy and moisture transport efficiency described in Sections 2.2.2 to 2.2.7 and assessed with regard to $R_n$ and $G$ in Section 3.1 on the potential evapotranspiration (PET) estimates for Forsmark, Norunda and Svartberget/Krycklan using the Penman (1948, 1956) and Penman-Monteith (Monteith 1965) equations is shown below in the following figures and tables.

- Figures 3-8, 3-9 and 3-10 show the annual variation in weekly average PET for the three sites based on the daily data aggregated from the years 2014–2016. In each panel, Penman (1948) based on the best available net radiation and ground heat flux is used as benchmark (red line) to which the other PET estimates are compared (blue lines). When available, observed ET (black lines and symbols) and other independent data are included in the plots for comparison.
- Table 3-3 show the mean annual PET for each tested model, and the ratio between the different models and the benchmark.

The following list provide a summary of the models and model names used in the assessment:

- **Penman-48,** Penman (1948) based on the best available $R_n$ and $G$ input (according to results in Section 3.1). Used as a benchmark to all other models in Figures 3-8, 3-9, 3-10, (a)–(i).
- **Penman-48***, Penman (1948) using $R_n$ and $G$ following Eriksson (1981), and is equivalent to how the Penman-SMHI is calculated (Figures 3-8a, 3-9a, 3-10a). The difference is that Penman-48* calculations are made with daily input data and Penman-SMHI is based on 30-minute input data and then averaged to daily mean PET values.
- **Penman-SMHI,** Penman (1948) as delivered by SMHI to SKB (Figures 3-8a, 3-9a, 3-10a).
- **Penman-56,** Penman (1956) using best available $R_n$ and $G$ (Figures 3-8b, 3-9b, 3-10b). The difference to Penman-48 is the parameters in the wind function (see Equation 2-7).
- **PM-FAO** and **PM-FAO****, FAO Reference Evapotranspiration using best available $R_n$ and $G$ (PM-FAO) or Rn and G following standard procedure by FAO (PM-FAO**) (Figures 3-8c, 3-9c, 3-10c).
- **PM-dual,** dual source implementation of the Penman-Monteith (Monteith 1965) as outlined in Section 2.1.4. and further described by Equations 2-15, 2-19, 2-25, 2-26, 2-27, 2-28, and 2-29. The dual source model is used with the best available Rn and G which are distributed to the canopy layer and the ground below, and subsequently used as input to the Penman-Monteith function with vegetation characteristics extracted from the ECOCLIMAP-SG database. The following PET-components are calculated with the dual-source model:
  - **PM-dual (tp),** potential transpiration from the vegetation layer (assuming dry vegetation (Figures 3-8e, 3-9e, 3-10e).
  - **PM-dual (ground),** potential evaporation from the ground (Figures 3-8f, 3-9f, 3-10f), that is soil evaporation or snow-evaporation depending on snow conditions.
  - **PM-dual (int),** potential evaporation of intercepted water assuming completely wet canopy surface (Figures 3-8e, 3-9e, 3-10e).
  - **PM-dual (tot),** the sum of PM-dual (tp) and PM-dual (ground) (Figures 3-8d, 3-9d, 3-10d), thus representing the potential evapotranspiration in conditions without intercepted water on the vegetation.
- **Jensen-Haise, S-HYPE, Priestley-Taylor:** PET estimated with the corresponding functions as described in Section 2. The Priestley-Taylor (Figures 3-8i, 3-9i, 3-10i) calculations are based on the best available $R_n$ and $G$ in the same way as Penman-48, Penman-56, PM-FAO and PM-dual. The Jensen-Haise (Figures 3-8g, 3-9g, 3-10g) and S-HYPE (Figures 3-8h, 3-9h, 3-10h) methods is using air temperature (and extra-terrestrial radiation) and are independent of the errors in estimating $R_n$ an $G$ identified in Section 3.1.

The results can be summarised as follows:

- Penman-48* results are similar to Penman-SMHI, which shows that the implementation of the calculations for this study are similar to the implementation used in the delivery to SKB.
- Both Penman-SMHI and Penman-48* exhibit up to 1 mm/day lower PET during summer, and somewhat lower values also during winter, compared to the benchmark (Figures 3-8a to 3-10a). This result is in line with the underestimation of the net radiation following Eriksson (1981) shown in Section 3.1.4. On average, PET calculated with Penman-SMHI and Penman-48* amount to 86 % and 84 %, respectively, of the benchmark PET (Table 3-3).
- The difference between the Penman (1948) and Penman (1956) wind functions is rather small (Figures 3-8b to 3-10b) compared to the impacts of the different net radiation estimates and the selection of PET formulas.
- The FAO reference evapotranspiration (PM-FAO) gives rather similar results as Penman-SMHI, especially during summer. This result illustrates that the underestimation of net radiation caused by using a constant albedo of 0.23 in PM-FAO is largely compensated for by the use of the Penman-Monteith (Monteith 1965) equations and parameters selected for the FAO reference crop (Allen et al. 1998). In fact, the average PET by the FAO reference evapotranspiration method is 84 % of the benchmark, which is identical to Penman (1948) using net radiation following Eriksson (1981).
- The Penman-Monteith equations (Monteith 1965) using the dual-source evapotranspiration model and land surface parameters from the ECOCLIMAP-SG database (PM-dual) generated PET values with a similar seasonal cycle but with lower values than the Penman (1948) benchmark and the FAO reference evapotranspiration (Figures 3-8d to 3-10d). The mean PET by the dual-source model is 66 % of the benchmark and 79 % of the estimates corresponding to Penman-SMHI.
- Furthermore, the dual-source PET model enables separating the evapotranspiration into transpiration and soil evaporation, and to estimate separately the potential evaporation of intercepted water (Figures 3-8e-f to 3-10e–f). The latter was in fact close to the Penman (1948) benchmark (Figure 3-8e to 3-10e), illustrating the difficulties of using a single potential evapotranspiration estimate for different evapotranspiration components in boreal forest ecosystems.
- The Jensen-Haise and S-HYPE functions (Section 2.1.3), being independent of the net radiation estimation issues, provide PET estimates with much smoother annual cycles and distinctive delays in the seasonal response compared to the different Penman and Penman-Monteith based estimates (Figures 3-8g–h to 3-10g–h). The Jensen-Haise equation, with the recommended standard parameters from Oudin et al. (2005) provided estimates that we similar to the dual-source model, while the S-HYPE model provided slightly lower values.

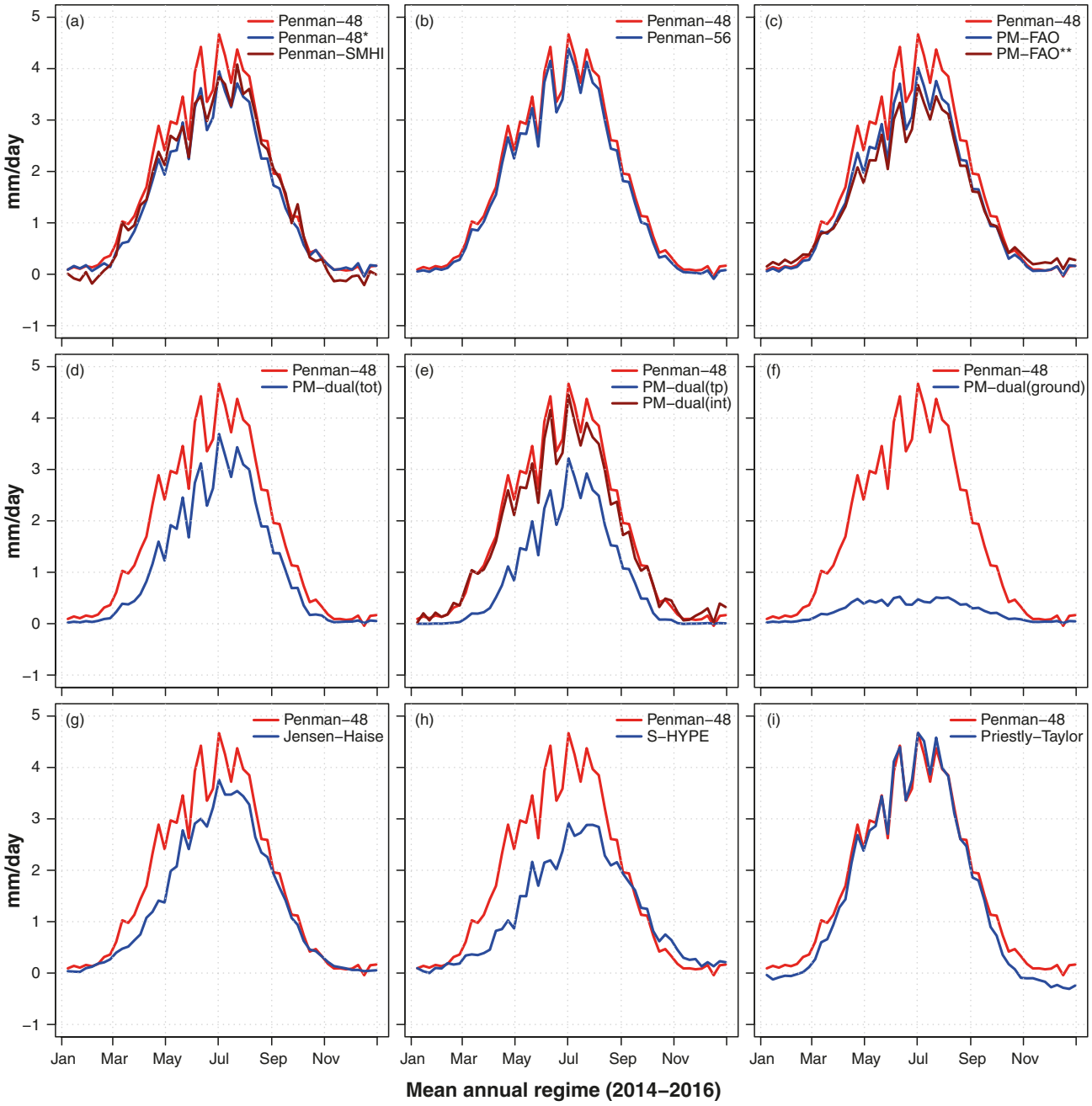


***Figure 3-8.*** *Potential evapotranspiration (PET) calculated for the Forsmark area with different PET-functions. In each sub-panel, Penman (1948) forced by revised $R_n$-G is used as a benchmark (Penman-48, red) and compared to: (a) Penman (1948) using Rn-G following Eriksson (1981) (Penman-48*, blue) and Penman (1948) as calculated by SMHI to SKB (Penman-SMHI, dark-red), (b) Penman (1956) using revised Rn-G (Penman-56, blue), (c) FAO Reference Evapotranspiration with revised $R_n$-G (PM-FAO, blue) and Rn-G following FAO (FAO-PM**, dark-red), (d)–(f) Dual-source application of the Penman-Monteith (Monteith 1965) using revised $R_n$-G and site-specific parameters from ECOCLIMAP-SG: (e) transpiration (PM-dual (tp)) and interception (PM-dual (int)), (f) soil/snow evaporation (PM-dual (ground)), (d) the sum of PM-dual (tp) and PM-dual (ground) (PM-dual (tot)), (g) Jensen-Haise McGuiness with parameters from Oudin et al. (2017), (h) Temperature index with seasonal delay, S-HYPE (Strömqvist et al. 2012), and (i) Priestley and Taylor (1972) with revised $R_n$-G. Time-series of daily data for the period 2014–2016 were aggregated to a mean annual regime at a weekly time resolution.*

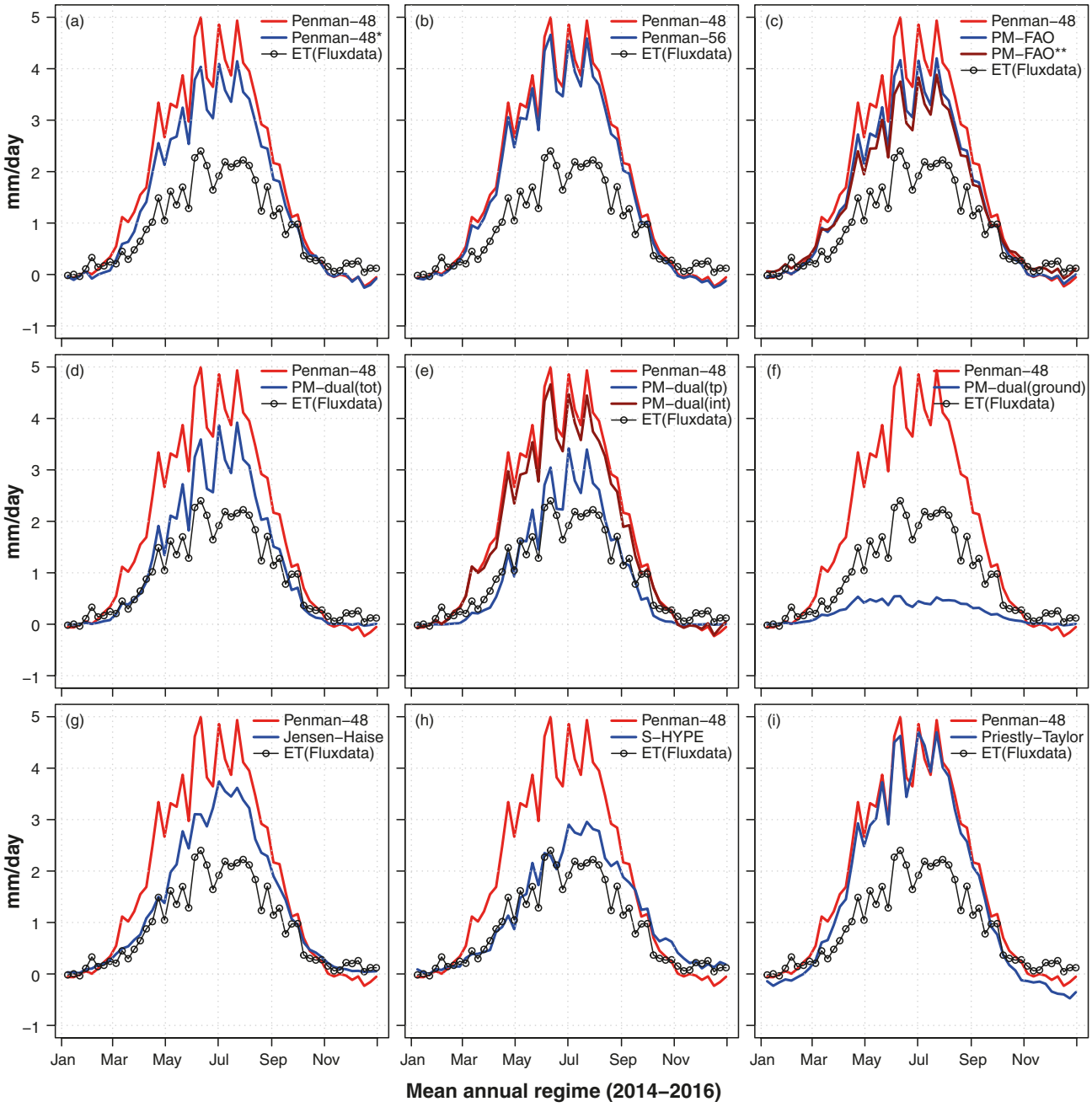


***Figure 3-9.*** *Similar plot as Figure 3-8 but for the Norunda area. In addition to the different PET functions, observed (actual) evapotranspiration from the ICOS flux-tower (black lines + symbols) is included in each panel.*

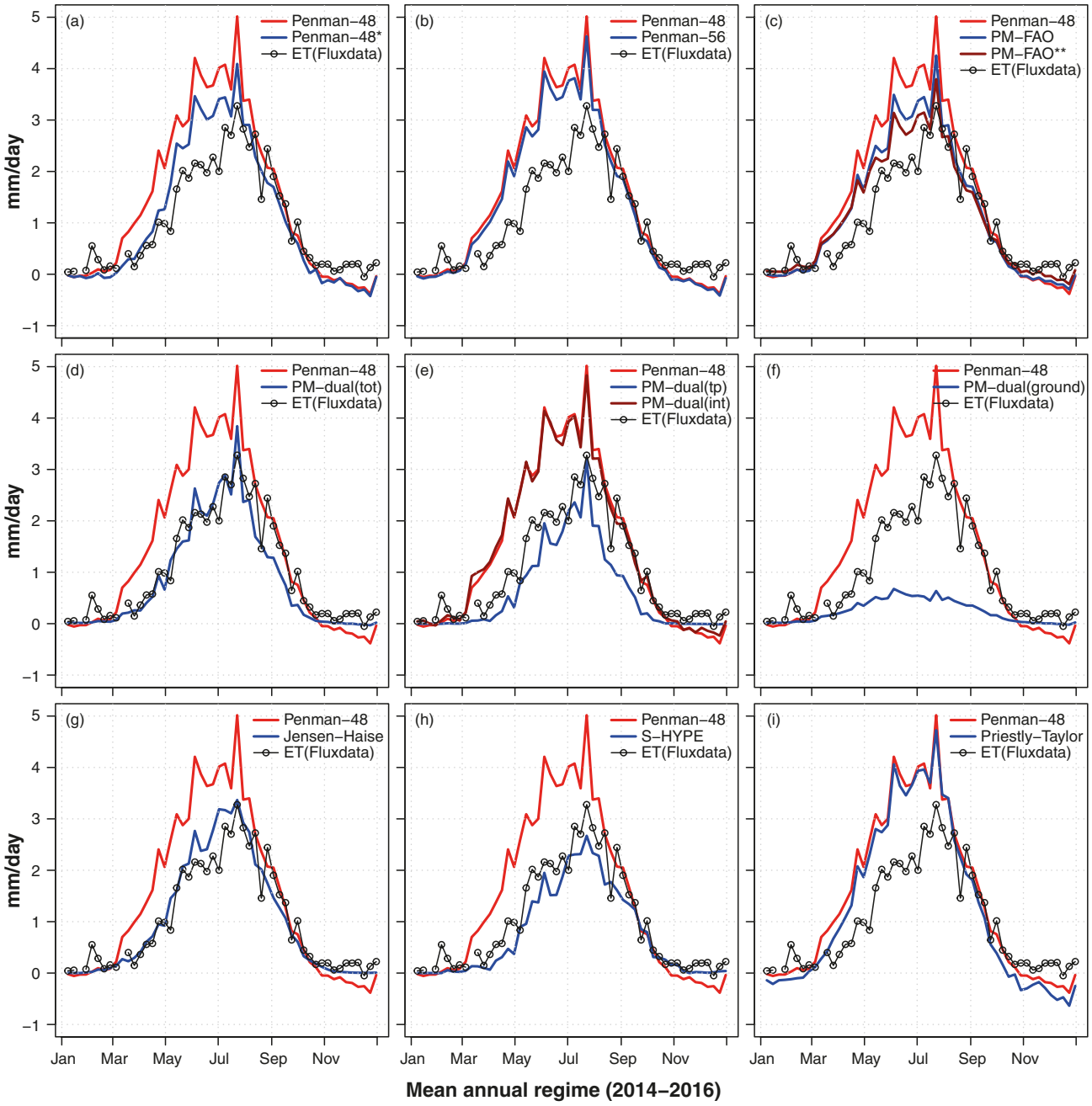


***Figure 3-10.*** *Similar plot as Figure 3-8 but for the Krycklan/Svartberget area. In addition to the different PET functions, observed (actual) evapotranspiration from the ICOS flux-tower (black lines + symbols) is included in each panel.*

**Table 3-3. Mean annual (2014–2016) potential evapotranspiration for the Forsmark area, estimated by different functions and input data combinations, given as mm/year and as a fraction of the different Penman-1948, FAO reference evapotranspiration, and dual-source Penman-Monteith estimates.**

| Model | mm/yr | f_PE-48* | f_PE-48 | f_PM-FAO* | f_PM-FAO | f_PM-dual |
|---|---|---|---|---|---|---|
| Penman-48 | 611 | 1.19 | 1.00 | 1.22 | 1.19 | 1.51 |
| Penman-56 | 562 | 1.10 | 0.92 | 1.12 | 1.09 | 1.38 |
| Priestley-Taylor | 552 | 1.08 | 0.90 | 1.10 | 1.07 | 1.36 |
| Penman-SMHI | 526 | 1.03 | 0.86 | 1.05 | 1.02 | 1.30 |
| PM-FAO | 516 | 1.01 | 0.84 | 1.03 | 1.00 | 1.27 |
| Penman-1948* | 512 | 1.00 | 0.84 | 1.02 | 0.99 | 1.26 |
| PM-FAO** | 500 | 0.98 | 0.82 | 1.00 | 0.97 | 1.23 |
| Jensen-Haise | 477 | 0.93 | 0.78 | 0.95 | 0.92 | 1.17 |
| S-HYPE | 409 | 0.80 | 0.67 | 0.82 | 0.79 | 1.01 |
| PM-dual (total) | 406 | 0.79 | 0.66 | 0.81 | 0.79 | 1.00 |
| PM-dual (transpiration) | 319 | 0.62 | 0.52 | 0.64 | 0.62 | 0.78 |
| PM-dual (ground) | 87 | 0.17 | 0.14 | 0.17 | 0.17 | 0.22 |
| PM-dual (interception) | 571 | 1.11 | 0.93 | 1.14 | 1.11 | 1.41 |

# 4 Conclusions and recommendations

## 4.1 Conclusions

The concept of potential evapotranspiration and different methods commonly used in the literature have been reviewed and analysed using data from three sites on a climatological gradient in Sweden: the SKB site in Forsmark and the two ICOS monitoring sites in Norunda and Svartberget/Krycklan.

The Penman (1948) equation as implemented by SMHI following Eriksson (1981) generated potential evapotranspiration that was about 26–30 % higher than a dual-source implementation of the Penman-Monteith equation (Monteith 1965) with parameter values representing the boreal landscape of the study areas, which confirms previous findings of an apparent overestimation of the potential evapotranspiration of this data when used as input to hydrological modelling of the Forsmark and Krycklan basins.

However, due to an underestimation of net radiation by the Eriksson (1981) method, the potential evapotranspiration data provided by SMHI to SKB was in fact close to the values obtained with the FAO reference evapotranspiration method (Allen et al. 1998) and about 14 % lower than estimates using the Penman (1948) equation when forced with corrected net radiation data.

The main reason for the apparent overestimation of the potential evapotranspiration at Forsmark and Krycklan was thus in the selection of the Penman (1948) equation, being representative for the evapotranspiration of a short-cut grass, instead of the Penman-Monteith equation with parameters for the land-surface control on water availability (stomata resistance), moisture transport in the atmosphere (aerodynamic resistances based on vegetation characteristics) and available energy (albedo and distribution of radiation between canopy and ground) relevant for a boreal forest landscape.

It was further shown how parameters for using the Penman-Monteith equation could be extracted from a global database of land-surface parameters (ECOCLIMAP-SG) developed for meteorological model applications, including satellite-based estimates of the leaf area index and tree heights.

## 4.2 Recommendations

It is highly recommended to adjust the estimation of net radiation used in the Penman-SMHI calculations. The implementation of the Brunt (1932) net longwave radiation equation used by SMHI gives too high values, leading to a general underestimation of the net radiation. Furthermore, the fixed albedo of 0.5 during snow-covered conditions is too high for forested areas, contributing to large underestimation of net radiation during the transition from winter to spring. The dual-source model may be a good alternative to estimate more correctly an effective albedo of forested areas, considering both the lower albedo of the trees and the higher albedo of the snow below. It is also recommended to estimate the presence of snow and the albedo of snow-covered ground with a model as used in this report. Observed snow depth can be used to replace or constraining the model estimates.

The ground heat flux in boreal forests was shown to be represented well by the Gardelin and Lindström (1997) model with the modifications suggested in this report. However, the investigation was limited to data from forested areas, and alternative solutions not tested here should be considered. It is recommended to re-assess the model with additional data, perhaps generated by more advanced models, before making changes to the currently used routine for other than forests.

Regarding the choice of PET equation, it is recommended to switch from the Penman (1948, 1956) to the Penman-Monteith equation (Monteith 1965), to enable the use of parameters adapted to boreal forests landscape characteristics. It is further suggested to adopt a dual-source framework for partitioning of the PET to the evaporation components (transpiration, soil/snow evaporation, and canopy evaporation). For simplicity, it may be enough to partition a single-source PET between the evaporation components using a similar approach as e.g. Hansen (1984). This would also make it possible to use alternative PET functions, such as the S-HYPE or Jensen-Haise methods for the single-source estimate. However, a more precise characterization of the differences in the response of the different

evaporation components to the meteorological conditions is only possible with a dual-source model where the forcing conditions are distributed to the different evaporating surfaces, to enable application of the PET calculations individually for each component.

For lake evaporation, which was not considered in this report, it is recommended to adopt a PET-method that represents the impact of the lake heat storage on the available energy for evaporation in a realistic way. The equilibrium temperature method (Edinger et al. 1968) as recommended by Finch and Hall (2001) may be a good option. A more simplified approach could be the temperature index method with seasonal delay as suggested in Rohde et al. (2006).

Finally, as the next step, it is recommended to test the impact of using the different PET estimates presented in this report as input to a hydrological model for the Forsmark and Krycklan basins. Depending on the hydrological model system, this may require some developments, for instance to enable to use of multiple PET input data, or alternative methods to distribute a single-source PET. In any case, it would be interesting to investigate for instance to what extent a dual-source PET would improve the calibration of the MIKE SHE model for Forsmark compared to a single-source, or to what extent the hydrological model results would be affected by the switch from Penman to Penman-Monteith based PET.

# References

SKB's (Svensk Kärnbränslehantering AB) publications can be found at www.skb.com/publications.


**Allen R G, Pereira L S, Raes D, Smith M, 1998.** Crop evapotranspiration – Guidelines for computing crop water requirements – FAO Irrigation and drainage paper 56. Rome: Food and Agriculture Organization of the United Nations. Available at: https://www.fao.org/3/x0490e/x0490e00.htm [13 September 2022].

**Bergström S, 1976.** Development and application of a conceptual runoff model for Scandinavian catchments. Norrköping, Sweden: SMHI. (SMHI rapporter, Hydrologi och oceanografi 7.)

**Bewley D, Essery R, Pomeroy J, Menard C, 2010.** Measurements and modelling of snowmelt and turbulent heat fluxes over shrub tundra. Hydrology and Earth System Sciences 14, 1331–1340.

**Blyth E M, Harding R J, Essery R, 1999.** A coupled dual source GCM SVAT. Hydrology and Earth System Sciences 3, 71–84.

**Bosson E, Gustafsson L-G, Sassner M, 2008.** Numerical modelling of surface hydrology and near-surface hydrogeology at Forsmark. Site descriptive modelling, SDM-Site Forsmark. SKB R-08-09, Svensk Kärnbränslehantering AB.

**Brandt M, Grahn G, 1998.** Avdunstning och avrinningskoefficient i Sverige, 1961–1990: beräkningar med HBV-modellen. Norrköping, Sweden: SMHI. (SMHI Hydrologi 73) (In Swedish.)

**Brunt D, 1932.** Notes on radiation in the atmosphere. Quarterly Journal of the Royal Meteorological Society 58, 389–420.

**CNRM, 2022.** ECOCLIMAP-SG. Available at: https://opensource.umr-cnrm.fr/projects/ecoclimap-sg/wiki [7 September 2022].

**Deardorff J W, 1978.** Efficient prediction of ground surface temperature and moisture, with inclusion of a layer of vegetation. Journal of Geophysical Research 83, 1889–1903.

**Doorenbos J, Pruitt W O, 1977.** Crop water requirements. Rome: FAO. (FAO Irrigation and Drainage Paper 24.)

**Druel A, Munier S, Mucia A, Albergel C, Calvet J-C, 2022.** Implementation of a new crop phenology and irrigation scheme in the ISBA land surface model using SURFEX_v8.1. Geoscientific Model Development 15, 8453–8471.

**Edinger J E, Duttweiler D W, Geyer J C, 1968.** The response of water temperature to meteorological conditions. Water Resources Research 4, 1137–1143.

**Eriksson B, 1981.** Den "potentiella" evapotranspirationen i Sverige. Norrköping, Sweden: SMHI. (SMHI rapporter, Hydrology and oceanography 27) (In Swedish.)

**ESA, 2017.** Land Cover CCI. Product user guide, version 2. Available at: http://maps.elie.ucl.ac.be/CCI/viewer/download/ESACCI-LC-Ph2-PUGv2_2.0.pdf

**Finch J W, Hall R, 2001.** Estimation of open water evaporation. R&D Technical Report W6-043/TR, Environment Agency, UK. Available at: https://www.gov.uk/government/publications/estimation-of-open-water-evaporation

**Gardelin M, Lindström G, 1997.** Priestley–Taylor evapotranspiration in HBV-simulations. Nordic Hydrology 28, 233–246.

**Gupta H V, Kling H, Yilmaz K K, Martinez G F, 2009.** Decomposition of the mean squared error and NSE performance criteria: Implications for improving hydrological modelling. Journal of Hydrology 377, 80–91.

**Gustafsson D, Lewan E, Jansson P-E, 2004.** Modeling water and heat balance of the boreal landscape – comparison of forest and arable land in Scandinavia. Journal of Applied Meteorology 43, 1750–1767.

**Halldin S, 1988.** Swedish evaporation research – A review. Hydrology Research 19, 303–340.

**Hansen S, 1984.** Estimation of potential and actual evapotranspiration. Nordic Hydrology 15, 1984, 205–212.

**Jensen M E, Haise H R, 1963.** Estimating evapotranspiration from solar radiation. Journal of the Irrigation and Drainage Division 89, 15–41.

**Johansson P-O, Öhman J, 2008.** Presentation of meteorological, hydrological and hydrogeological monitoring data from Forsmark. Site descriptive modelling, SDM-Site Forsmark. SKB R-08-10, Svensk Kärnbränslehantering AB.

**Jutebring Sterte E, Johansson E, Sjöberg Y, Huseby Karlsen R, Laudon H, 2018.** Groundwater-surface water interactions across scales in a boreal landscape investigated using a numerical modelling approach. Journal of Hydrology 560, 184–201.

**Laudon H, Taberman Ågren A, Futter M, Ottosson-Löfvenius M, Bishop K, 2013.** The Krycklan Catchment Study – A flagship infrastructure for hydrology, biogeochemistry and climate research in the boreal landscape. Water Resources Research 49, 7154–7158.

**Le Moigne P (ed), 2018.** SURFEX Scientific documentation. Available at: http://www.umr-cnrm.fr/surfex/IMG/pdf/surfex_scidoc_v8.1.pdf [13 September 2022].

**Lindroth A, Lagergren F, Aurela M, Bjarnadottir B, Christensen T, Dellwik E, Grelle A, Ibrom A, Johansson T, Lankreijer H, Launiainen S, Laurila T, Mölder M, Nikinmaa E, Pilegaard K, Sigurdsson B D, Vesala T, 2008.** Leaf area index is the principal scaling parameter for both gross photosynthesis and ecosystem respiration of Northern deciduous and coniferous forests. Tellus B: Chemical and Physical Meteorology 60, 129–142.

**Lindström G, Gardelin M, Persson M, 1994.** Conceptual modelling of evapotranspiration for simulations of climate change effects. Norrköping, Sweden: SMHI. (SMHI Reports, Hydrology 10.)

**Lindström G, Pers C, Rosberg J, Strömqvist J, Arheimer B, 2010.** Development and testing of the HYPE (Hydrological Predictions for the Environment) water quality model for different spatial scales. Hydrology Research 41, 295–319.

**Löfgren A (ed), 2010.** The terrestrial ecosystems at Forsmark and Laxemar-Simpevarp. SR-Site Biosphere. SKB TR-10-01, Svensk Kärnbränslehantering AB.

**Masson V, Champeaux J, Chauvin F, Meriguet C, Lacaze R, 2003.** A global database of land surface parameters at 1-km resolution in meteorological and climate models. Journal of Climate 16, 1261–1282.

**McGuinness J L, Bordne E F, 1972.** A comparison of lysimeter-derived potential evapotranspiration with computed values. Technical Bulletin 1452, Agricultural Research Service, U.S. Department of Agriculture.

**McMahon T A, Peel M C, Lowe L, Srikanthan R, McVicar T R, 2013.** Estimating actual, potential, reference crop and pan evaporation using standard meteorological data: a pragmatic synthesis. Hydrology and Earth System Sciences 17, 1331–1363.

**Menard C B, Essery R, Pomeroy J, 2014.** Modelled sensitivity of the snow regime to topography, shrub fraction and shrub height. Hydrology and Earth System Sciences 18, 2375–2392.

**Monteith J L, 1965.** Evaporation and environment. Symposia of the Society for Experimental Biology 19, 205–234.

**Mölder M, Grelle A, Lindroth A, Halldin S, 1999.** Flux-profile relationships over a boreal forest – roughness sublayer corrections, Agricultural and Forest Meteorology 98–99, 645–658.

**Mölder M, Kljun N, Lehner I, Båth A, Holst J, Linderson M, 2022.** ETC L2 Meteo, Norunda, 2017-12-31–2021-12-31. ICOS RI. Available at: https://hdl.handle.net/11676/eJZwR_ipYxZPPGhNy3p8u3Df

**Oudin L, Hervieu F, Michel C, Perrin C, Andréassian V, Anctil F, Loumagne C, 2005.** Which potential evapotranspiration input for a lumped rainfall–runoff model? Part 2 – Towards a simple and efficient potential evapotranspiration model for rainfall–runoff modelling. Journal of Hydrology 303, 290–306.

**Peichl M, Nilsson M, Smith P, Marklund P, De Simon G, Löfvenius P, Dignam R, Holst J, Mölder M, Andersson T, Linderson M, Lindgren K, Ottosson-Löfvenius M, Tülp H, Öquist M, 2022.** ETC L2 Fluxes, Svartberget, 2018-12-31 – 2021-12-31. ICOS RI. Available at: https://hdl.handle.net/11676/miQUqRWBDc7jnmJmzSXi8lT7

**Penman H L, 1948.** Natural evaporation from open water, bare soil and grass. Proceedings of the Royal Society A 193, 120–146.

**Penman H L, 1956.** Evaporation: an introductory survey. NJAS 4, 9–29.

**Priestley C H B, Taylor R J, 1972.** On the assessment of surface heat flux and evaporation using large-scale parameters. Monthly Weather Review 100, 81–92.

**Purdy A J, Fisher J B, Goulden M L, Famiglietti J S, 2016.** Ground heat flux: An analytical review of 6 models evaluated at 88 sites and globally. Journal of Geophysical Research: Biogeosciences 121, 3045–3059.

**Rasmus S, Gustafsson D, Koivusalo H, Laurén A, Grelle A, Kauppinen O-K, Lagnvall O, Lindroth A, Rasmus K, Svensson M, Weslien P, 2013.** Estimation of winter leaf area index and sky view fraction for snow modelling in boreal coniferous forests: consequences on snow mass and energy balance. Hydrological Processes 27, 2876–2891.

**Rohde A, Lindström G, Rosberg J, Pers C, 2006.** Grundvattenbildning i svenska typjordar – översiktlig beräkning med en vattenbalansmodell. Report Series A 66. Uppsala University. Available at: https://www.sgu.se/globalassets/grundvatten/grundvattennivaer/grundvattenbildning/rodhe-et-al_2006.pdf (In Swedish.)

**Savenije H H G, 2004.** The importance of interception and why we should delete the term evapotranspiration from our vocabulary. Hydrological Processes 18, 1507–1511.

**Shuttleworth W J, 1993.** Evaporation. In Maidment D R (ed). Handbook of hydrology. New York: McGraw-Hill, Chapter 4.

**Shuttleworth W J, Wallace J S, 1985.** Evaporation from sparse crops – an energy combination theory. Quarterly Journal of the Royal Meteorological Society 111, 839–855.

**Silversides R H, 1978.** Forest and airport wind speeds. Atmosphere-Ocean 16, 293–299.

**Stigter C J, 1980.** Assessment of the quality of generalized wind functions in Penman's equations. Journal of Hydrology 45, 321–331.

**Strömqvist J, Arheimer B, Dahné J, Donnelly C, Lindström G, 2012.** Water and nutrient predictions in ungauged basins: set-up and evaluation of a model at the national scale. Hydrological Sciences Journal 57, 229–247.

**Stähli M, Jonas T, Gustafsson D., 2009.** The role of snow interception in winter-time radiation processes of a coniferous sub-alpine forest. Hydrological Processes 23, 2498–2512.

**Thornthwaite C W, 1948.** An approach toward a rational classification of climate. Geographical Review 38, 55–94.

**Verseghy D L, McFarlane N A, Lazare M, 1993.** CLASS–A Canadian land surface scheme for GCMs, II. Vegetation model and coupled runs. International Journal of Climatology 13, 347–370.

**Werner K, Sassner M, Johansson E, 2013.** Hydrology and near-surface hydrogeology at Forsmark – synthesis for the SR-PSU project. SR-PSU Biosphere. SKB R-13-19, Svensk Kärnbränslehantering AB.

**Werner K, Norville J, Öhman J, 2014.** Meteorological, hydrological and hydrogeological monitoring data from Forsmark – compilation and analysis for the SR-PSU Project. SR-PSU Biosphere. SKB R-13-20, Svensk Kärnbränslehantering AB.

# Appendix A

# Summary of input data and calculation methods

## A1 Input variable requirements summary table

**Table A-1. Input variable requirements for Penman and Penman-Monteith.**

| Symbol | Variable | Usage | Primary data source* |
|---|---|---|---|
| $T_a$ | Air temperature | Proxy for available energy, and/or used as input to estimate other variables, ie. $R_n$, $e_s$, $e_a$, $\Delta$, $\gamma$, $\rho$. | Meteorological input data. |
| RH | Relative humidity | To estimate actual vapour pressure if missing from observations. | Meteorological input data. |
| $p_a$ | Air pressure | Calculations related to transformation from vapour pressure to water mass. | Meteorological input data, or assumed constant pressure 101.3 kPa. |
| $R_g$ | Global radiation | To estimate net radiation ($R_n$). | Meteorological input data or derived from atmospheric turbidity, cloudiness and extraterrestrial radiation. |
| $u_{10m,}$ $u2_m$ | Windspeed at 10 m and 2 m height | Input to the Penman wind-functions and to the function for aerodynamic resistance ($r_a$). | Meteorological input ($u_{10m}$) or derived from $u_{10m}$ (Equation 2-22). |
| $e_a$ | Actual vapour pressure | vapour pressure deficit (transport efficiancy), net radiation (available energy). | Derived from $T_a$ and RH (Equation A-3). |
| $e_s$ | saturation vapour pressure | vapour pressure deficit (transport efficiancy). | Derived from $T_a$ (Equation A-1). |
| $\Delta$ | Slope of saturation vapour pressure temperature dependence | Key for the derivation of the Penman equation, necessary to eliminate dependence on surface conditions. | Derived from $T_a$ (Equation A-2). |
| $\gamma$ | Psychrometer constant | Parametet needed for the transformation of latent heat flux into moisture flux. | Derived from Pa and $\lambda$ (Equation A-7). |
| $R_n$ | Net radiation | Available energy for evapotranspiraiton. | Derived from $R_g$, $\alpha$, $T_a$, and ea (Equation 2-14) or part of meteorological input data. |
| G | Ground heat flux | Available energy for evapotranspiraiton. | Derived from $R_n$ (Equation 2-20). |
| $r_a$ | Aerodynamic resistance** | Vapour transport efficiency from evaporating surface to the atmosphere. | Derived from wind speed and surface roughness for momentum and heat (Equations 2-24 to 2-28; Table 2-4). |
| $r_s$ | Surface resistance** | Vapour transport efficiency at the evaporating surface. | Constant or derived as function of land surface characteristics (Equations 2-29 to 2-33; Table 2-4). |

**only used in Penman-Monteith equation.

## A2 Calculation of various atmospheric parameters

### A2.1 Saturation vapour pressure

Several equations have been suggested for the saturation vapour pressure temperature function. The following function is recommended by FAO (Allen et al. 1998) and provides the saturation pressure in kPa:

$$e_s = 0.6108 \times \exp\left(\frac{17.27 \times T_a}{(T_a + 237.3)}\right)$$ Equation A-1

### A2.2 Slope of the saturation vapour pressure function

The slope of the saturation pressure function, Δ (kPa/C), is a key element of the Penman and Penman-Monteith equations, here based on Equation A-1:

$$\Delta = \frac{4098}{(T_a + 237.3)^2} \times 0.6108 \times \exp\left(\frac{17.27 \times T_a}{(T_a + 237.3)}\right)$$ Equation A-2

### A2.3 Actual vapour pressure

The actual vapour pressure, $e_a$ (kPa) can be estimated from air temperature $T_a$ (C) and relative humidity $RH$ (%) using the saturation vapour pressure function (Equation A-1):

$$e_a = e_s(T_a) \times RH \times 0.01$$ Equation A-3

### A2.4 Specific humidity

Specific humidity $q$ (kg/kg) is the mass fraction of water vapour in the air (the ratio of the water vapour mass to the total mass of the air in an air parcel). It can be approximated using the mixing ratio $MR$ according to:

$$MR = 0.622 \times \frac{e_a}{p_a - e_a}$$
$$q = \frac{MR}{1 + MR}$$ Equation A-4

where $e_a$ is the actual vapour pressure (Equation A-3) and $p_a$ is the air pressure (kPa). If the air pressure is not available it can be approximated by the standard pressure 101.3 kPa. The value 0.622 is the ratio of the molecular weights of water vapour and dry air, respectively

### A2.5 Latent heat of vaporization and sublimation

The latent heat of vaporization $\lambda$ (MJ $kg^{-1}$) is the amount of heat needed to transform 1 kg of liquid water to water vapour by evaporation, and is one of the parameters in the Penman and Penman-Monteith equations. It has a value of about 2.5 MJ $Kg^{-1}$, but more accurate estimation is obtained if a small temperature dependence is also considered:

$$\lambda = 2.5008 - 0.002361 \times T_a$$ Equation A-5

The corresponding latent heat for sublimation $\lambda_s$ (phase change from ice to water vapour) is slightly higher, approximately 2.83 MJ $Kg^{-1}$, and is described by the following temperature function:

$$\lambda_s = 2.8341 - 0.00029 \times T_a$$ Equation A-6

### A2.6 Psychrometric constant

The psychrometric constant expresses the ratio of specific heat of moist air to the latent heat of vaporization:

$$\gamma = \frac{c_p p_a}{0.622\lambda}$$ Equation A-7

where $c_p$ = 0.001013 MJ kg$^{-1}$ K$^{-1}$ is the specific heat of moist air at constant pressure, $P_a$ is the air pressure (kPa), and $\lambda$ (MJ kg$^{-1}$)) is the latent heat of vaporization, and 0.622 is the ratio of the molecular weights of water vapour and dry air, respectively.

### A2.7 Extra-terrestrial radiation

Daily average extra-terrestrial radiation is calculated with the following procedure, following the equations provided in the FAO crop evapotranspiration guidelines (Allen et al. 1998):

The inverse relative distance between the Earth and the Sun $d_r$ and the solar declination $\delta$ is calculated from the day number of the year $J$ (1 to 365):

$$d_r = 1 + 0.033cos\left(\frac{2\pi}{365}J\right)$$ Equation A-8

$$\delta = 0.409sin\left(\frac{2\pi}{365}J - 1.39\right)$$ Equation A-9

Based on the declination and latitude *lat* (in radians), the cosine of the sunset hour angle *cos(ω)* is calculated as:

$$\cos(\omega) = -tan(lat)\tan(\delta)$$ Equation A-10

which is transformed to sunset hour angle ω (in radians) according to:

$$\omega = \begin{cases} 0 & \cos(\omega) \geq 1 \\ \arccos(\cos(\omega)) & -1 < \cos(\omega) < 1 \\ \pi & \cos(\omega) \leq -1 \end{cases}$$ Equation A-11

Finally, if the sunset hour w > 0 then the extra-terrestrial radiation $R_{ext}$ (MJ m$^{-2}$ d$^{-1}$) is calculated as:

$$R_{ext} = \frac{1440}{\pi} G_{sc} d_r \left(\omega \sin(lat)\sin(\delta) + cos(lat)cos(\delta)sin(\omega)\right)$$ Equation A-12

where $G_{sc}$ is the solar constant (0.0820 MJ m$^{-2}$ min$^{-1}$), otherwise $R_e$ is set to 0.

Allen et al. (1998) also provide the equations to derive extra-terrestrial radiation for sub-daily time resolution.

### A2.8 Atmospheric turbidity and cloudiness

The atmospheric turbidity is defined as the ratio of the global radiation (downward shortwave radiation at the surface of the Earth) and the extra-terrestrial radiation (downward shortwave radiation at the top of the atmosphere ($\tau = R_s/R_{ext}$). The so-called Ångström formula relates the turbidity to the cloudiness C (-) according to:

$$\frac{R_s}{R_{ext}} = \left(a_s + b_s(1 - C)\right)$$ Equation A-13

where $a_s$ and $b_s$ are coefficients that will vary depending on atmospheric conditions such as humidity and dust as well as the solar angle above the horizon. If measured global radiation and cloudiness data is available, site-specific values can be found by calibration. Standard values suggested by FAO (Allen et al. 1998) are $a_s$ = 0.25 and $b_s$ = 0.50, which can be interpreted as the maximum turbidity ($a_s + b_s$) is around 0.75 and the minimum turbidity ($a_s$) is around 0.25.

Eriksson (1981) used the Ångström formula to estimate global radiation as a function of observed cloudiness. However, the relationship can also be used to estimate cloudiness from measured global radiation, since the cloudiness is an important input data to the net radiation estimation. Eriksson further used seasonal estimates of the minimum and maximum turbidity. Thus, following Eriksson (1981) the calculation procedure used to produce the Penman-SMHI was using $a_s$ = 0.22, $b_s$ = 0.59 (April–September), $a_s$ = 0.15, $b_s$ = 0.62 (October–March), corresponding to a shift between winter and summer in the minimum and maximum turbidity from 0.15 to 0.22, and from 0.77 and 0.81 respectively.

FAO (Allen et al. 1998) further recommend an equation to estimate the increase in clear-sky turbidity as a function of solar angle and pollution, which might be important at high latitudes when the increase pathway through the atmosphere may further reduce the global radiation without impacts of clouds. The equation is an application of the so-called Beer's law, which is also used for the transmission of radiation through vegetation canopies:

$$a_s + b_s = exp\left(\frac{-0.0018P_a}{K_t sin(\phi)}\right)$$ Equation A-14

where $P_a$ is the atmospheric pressure (kPa), $f$ is the angle of the sun above the horizon (radians), and $K_t$ is a turbidity coefficient with values 1 for clean air and 0 for extremely polluted air.

## A3 Snow and snow albedo modelling

In order to obtain a consistent daily dataset of the presence of snow and of the albedo of the snow-covered ground, a simple day-degree snow model was used to simulate the evolution of the snow cover and its depth and albedo for the 3 study areas.

Snow mass is simulated as an integration over time of the daily snow fall (SF) and snow melt (M). Precipitation is separated into rainfall at air temperatures above +2 ºC, snowfall at air temperature below 0 ºC, and as mix of snowfall and rainfall in the temperature range between 0 ºC and +2 ºC, with the fraction of snowfall increasing linearly from the upper to lower temperature limit. The snow melt is calculated using the degree day function, as a linear function of air temperature, with the degree day factors adopted from Johansson and Öhman (2008). The snow mass is transformed into snow depth using a snow age dependent density function, adopted from Lindström et al. (2010). A snow age dependent function is also used to calculate the snow surface albedo, which decrease exponentially from a maximum value of 0.9 for fresh snow to 0.4 for old snow. The snow depth is used to adjust the calculations of the aerodynamic resistance, considering the change in surface roughness caused by the gradual covering of vegetation by the snow. This effect is of course very small for forests, where it can be ignored.

The simulated snow depths for the three study areas are compared with observed snow depths in Figure A-1.

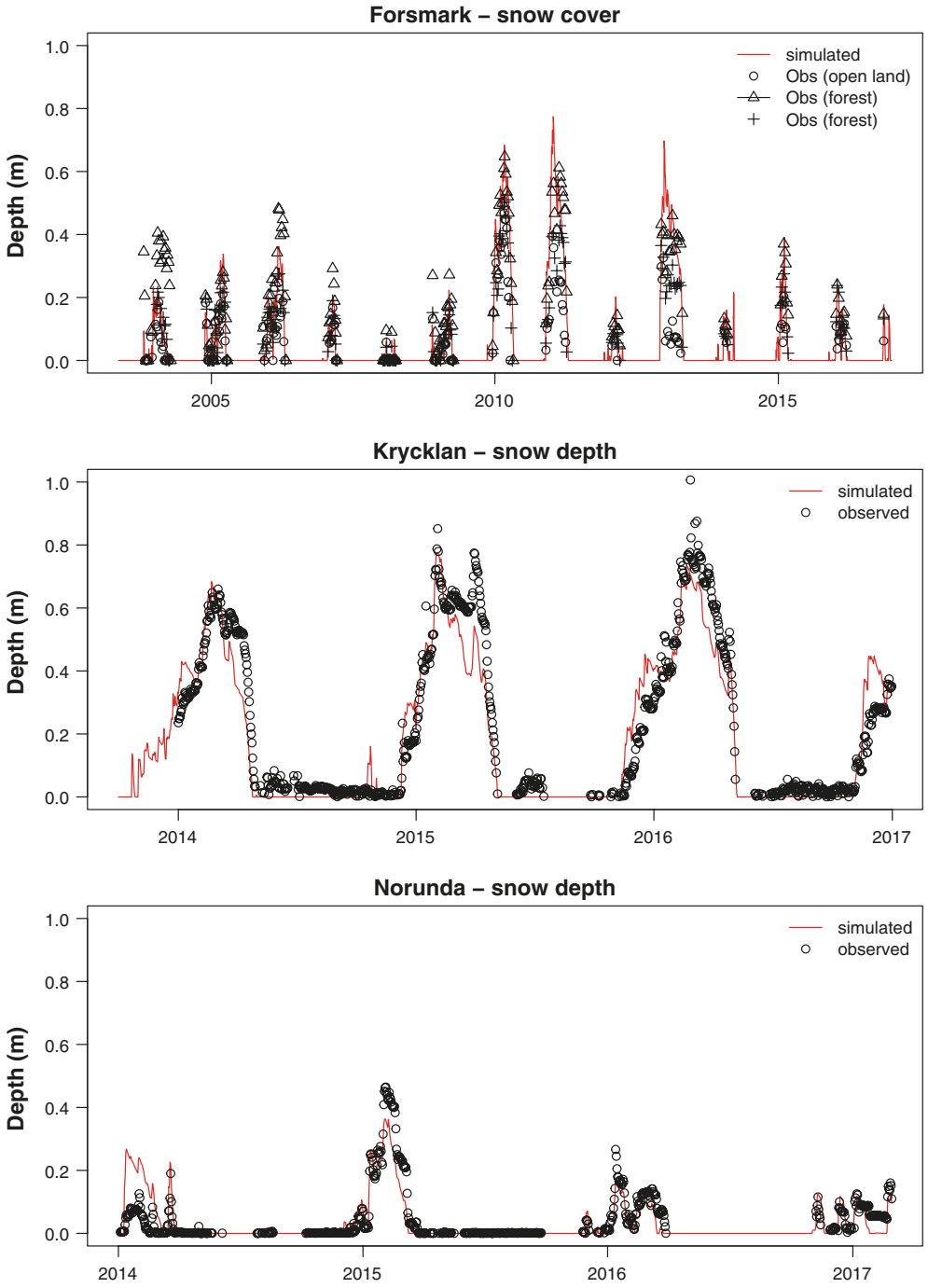


***Figure A-1.*** *Snow depth simulated for the study areas in Forsmark, Norunda and Svartberget/Krycklan compared to observations.*

Arkitektkopia AB, Bromma, 2023

SKB is responsible for managing spent nuclear fuel and radioactive waste produced by the Swedish nuclear power plants such that man and the environment are protected in the near and distant future.

**skb.se**